Physical Processes in Magnetically Driven Flares on the Sun, Stars, and Young Stellar Objects

Arnold O. Benz[1] and Manuel Güdel[1,2]

[1]Institute of Astronomy, ETH Hönggerberg, CH-8093 Zurich, Switzerland; email: benz@astro.phys.ethz.ch

[2]Department of Astronomy, University of Vienna, A-1180 Austria; email: guedel@astro.phys.ethz.ch

Annu. Rev. Astron. Astrophys. 2010. 48:241–87

First published online as a Review in Advance on April 26, 2010

The *Annual Review of Astronomy and Astrophysics* is online at astro.annualreviews.org

This article's doi: 10.1146/annurev-astro-082708-101757

0066-4146/10/0922-0241$20.00

Key Words

coronal heating, ionization of protoplanetary disks and atmospheres, magnetic reconnection, multiwavelength flare observations, particle acceleration

Abstract

The first flare on the Sun was observed exactly 150 years ago. During most of the long history, only secondary effects have been noticed, so flares remained a riddle. Now the primary flare products, high-energy electrons and ions, can be spatially resolved in hard X-rays (HXRs) and gamma rays on the Sun. Soft X-rays (SXRs) are observed from most stars, including young stellar objects. Structure and bulk motions of the corona are imaged on the Sun in high temperature lines and are inferred from line shifts in stellar coronae. Magnetic reconnection is the trigger for reorganization of the magnetic field into a lower energy configuration. A large fraction of the energy is converted into nonthermal particles that transport the energy to higher density gas, heating it to SXR-emitting temperatures. Flares on young stars are several orders of magnitude more luminous and more frequent; they significantly ionize protoplanetary disks and planetary ionospheres.

1. INTRODUCTION

Young stellar objects (YSOs): range from the very early phase of star formation of deeply embedded protostars, class 0, having an age of less than 10 years, up to weak-lined T Tauri stars, class III, with ages of several million years

Coronal mass ejections (CMEs): up to some 10^{16} g of coronal gas is expelled, driven, and contained by the magnetic field

Flares on the Sun, stars, and in young stellar objects (YSOs) are generally interpreted as signatures of magnetic energy suddenly released by reconnection. Recent interest in flares originates from their physical and chemical impact in the early phases of star and planet formation. Comparing solar and young stellar flares, the latter produce UV and X-ray emissions more powerful and frequent by many orders of magnitude. The ionizing radiation emitted by flares affects the degree of ionization in accretion disks of YSOs, thus controlling accretion, evaporation, disk chemistry, and the early planetary formation processes. Flare radiation and particles also heat and ionize outer planetary atmospheres, thus modifying their chemical evolution and contributing to atmospheric loss mechanisms.

Flares are the largest explosions in the Solar System rivaled only by coronal mass ejections (CMEs), another way to release magnetic energy related to reconnection but not the focus of this review. Even for the Sun, the magnetic geometry and physical processes impulsively releasing energy are more difficult to disentangle than was believed just a decade ago. Nevertheless, a suite of new instruments observing flares from radio waves to gamma rays and recording solar high-energy particles in situ has greatly contributed to our physical understanding of solar and stellar flares in the past decade. We mention, in particular, recent progress owing to observations of high-energy phenomena from the ground and, most dramatically, from space.

The physical principle of flares is simple and ubiquitous: Magnetic energy builds up by a dynamo process based on $\nabla \times (\mathbf{V} \times \mathbf{B})$ motions. It is subsequently annihilated, reconnecting the magnetic field to a less energetic configuration. Reconnection is not necessarily associated with a flare. Only its impulsive version in tenuous plasma hosts the many secondary and tertiary phenomena from particle acceleration and propagating beams to plasma heating and evaporation at the footpoints of the involved magnetic fields in the dense chromosphere below. These phenomena produce short, but often extremely bright radiations at all wavelengths.

Reconnection is a universal process and occurs in many places, from the Earth's magnetotail to the intergalactic plasma in clusters of galaxies. However, the conditions being widely dissimilar, the relevant processes at work may not be the same everywhere. As far as stars are concerned, a strong physical relationship is assumed between flares in stellar coronae such as the Sun's, where individual processes can be observed in some detail, and in highly active stars and YSOs where, however, additional processes and geometries are involved.

There is no standard flare model yet, not even for the Sun. This is different from the situation in elementary particle physics, where a large majority of observations accurately fit into one single picture, and this has been the state of affairs since the 1970s. The reasons for this deficiency are the uncertainty in the primary energy release in flares—the various circumstances and the multitude of processes that interact in the energy release and its final dissipation. Nevertheless, it is possible to discuss basic processes that have become better understood in recent years.

This review addresses physical processes in flares, their origin, and their subsequent effects in and around the Sun and Sun-like stars, including stars in their formation process interacting with their complex environments. We highlight new developments and trends in our physical understanding since the 1990s based on new observational capabilities. We do not aim to discuss the flare phenomenon comprehensively in all its facets. Specifically, we do not address in detail the overall physical and geometric properties of flares (e.g., statistics of peak temperatures, decay timescales, flaring loop lengths, densities and volumes inferred from light curves or spectroscopy, flaring active-region sizes, emission measure distributions, etc.), nor the methodology available to derive such parameters except in the context of our topics mentioned above. Also, discussions of the emission mechanisms (important particularly in the radio domain) are not in the spotlight

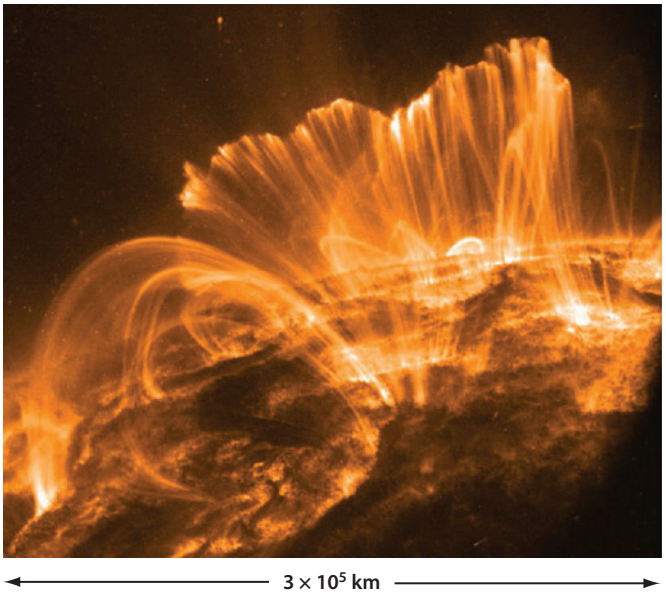

Figure 1

Transition Region and Coronal Explorer (TRACE) image of solar postflare loops in the FeIX EUV line at 171 Å. The emission outlines a magnetic arcade that produced an M-class flare (i.e., a medium-sized flare). The plasma temperature corresponds to 1–2 MK. The width of the figure is 3×10^5 km. (Credit: NASA.)

of this review. There is a vast amount of literature addressing and summarizing these issues. We refer the interested reader to Aschwanden (2002) and Benz (2008) for general reviews of solar flare observations and their characteristic physical properties, to Bastian, Benz & Gary (1998) for a review of solar radio flares and their emission mechanisms, to Krucker et al. (2008) for a summary of solar X-rays, and to Fletcher & Warren (2003) for extreme UV (EUV) flares. On the stellar side, Favata & Micela (2003), Güdel (2004), and Güdel & Nazé (2009) summarized stellar X-ray and EUV flares, their spectroscopic signatures and their physical parameters, and Güdel (2002) has reviewed flaring and quiescent stellar radio emission. The older solar and stellar literature on the flare phenomenon has been comprehensively described by Haisch, Strong & Rodono (1991).

We start our overview with flare-related brightenings observed by new instrumentation at many wavelengths and originating in various Sun-like stars and the Sun itself. In Section 3, general properties are reviewed as derived from a large number of flares. New insights in basic physical processes are presented in Section 4, and effects resulting from flares are discussed in Section 5.

2. GENERAL FLARE OBSERVATIONS

2.1. Solar Flares

When large amounts of magnetic energy build up in the corona, the process is necessarily related to magnetic fields in the photosphere, where the coronal field lines are anchored (**Figure 1**). Thus, solar flares, releasing substantial amounts of energy, are observed above and near concentrations of the photospheric magnetic field such as active regions (sunspots). When energy is discharged in the corona, accelerated particles and thermal conduction transport the energy preferentially along field lines back to the chromosphere and into interplanetary space. Accordingly, all atmospheric layers are affected by a large flare. Brightenings are observed in the photosphere, chromosphere, or corona, but occur in different wavelengths from radio waves to gamma rays. The brightenings at different wavelengths may originate from different radiation processes and are not necessarily

Extreme UV (EUV): defined by the wavelength range from 10 nm to 912 nm or by photon energies from 13.6 eV to 124 eV

simultaneous or cospatial. Although causally related, transport between the layers may substantially delay some phenomena.

Hard X-rays (HXRs): photons with energies between 10 keV and 500 keV; gamma rays are above 500 keV

Thermal emission: emitted by thermal electrons or ions; in regular flares, soft X-rays with energies below 10 keV are mostly thermal

Reconnection converts magnetic energy into kinetic particle energy and bulk plasma motion. The energy in nonthermal electrons and ions can be estimated from hard X-rays (HXRs) and gamma-ray line emissions, respectively. Most of the released energy is finally thermalized and radiated away as thermal emission in soft X-rays (SXRs) from the corona, UV line emission from the chromosphere and the (chromosphere/corona) transition region, and white light (optical continuum) from the lower chromosphere or photosphere. Radio and millimeter emissions are energetically negligible, but are important tracers. For these reasons, imaging observations at high temporal resolution at all wavelengths are useful for diagnostics and essential to shed light onto the intricate processes at play.

Solar flares occur at many sizes. The largest reported energies have been claimed to be a few times 10^{34} erg (Kane et al. 2005). Such estimates consider only the X-ray emission by nonthermal electrons with energies >20 keV, which are assumed to hit a cold thick target. Flares of this size occur on the Sun only in the maximum phase of magnetic activity, and even then, less than once per year. The smallest flares in active regions yet reported have energies below 10^{26} erg (Hannah et al. 2008). A large number of even smaller flares have been discovered outside of active regions at the boundaries of the quiet-Sun network, where magnetic flux is concentrated (Krucker et al. 1997). And even smaller flares have been found between network boundaries. They range down to the instrumental limit at thermal energies of a few times 10^{23} erg in the EUV (Parnell & Jupp 2000).

For the first time, the *Ramaty High-Energy Solar Spectroscopic Imager* (RHESSI) (Lin et al. 2002), launched in 2002, is providing flare images at HXRs above 100 keV up to gamma rays. Thus, RHESSI has closed this important gap in solar flare observations. Its impact has been augmented by high spectral resolution, allowing the separation of thermal emission from nonthermal emission (see **Figure 2**). Similarly, the *Hinode* spacecraft (Kosugi et al. 2007), launched in 2006, has dramatically improved flare imaging in SXRs (<3 keV), coronal EUV lines forming at temperatures up to 20 million K (MK), and white light at 0.2-arcsec spatial resolution. X-ray imaging is often presented in the context of EUV observations of the plasma at lower temperature, typically 1 MK, where the *Transition Region and Coronal Explorer* (TRACE) satellite has provided images at 1-arcsec resolution (Handy et al. 1999). Imaging at high spatial and temporal resolution will soon make a further step with the *Solar Dynamics Observatory* (SDO) observing simultaneously variations in the photosphere, chromosphere, and corona in unprecedented detail.

Most important for future studies are the new capabilities to combine imaging observations at different wavelengths. An example is displayed in **Figure 3**, showing emissions in HXR, SXR, and radio waves. The combination of three wavelengths demonstrates that the flaring SXR loop is accompanied by a coronal HXR source at the top and by a footpoint in HXR at low altitude (a second footpoint source may be located behind the limb). In most flares, some of the several kinds of nonthermal radio emissions appear at the higher altitudes above the loop.

2.2. Stellar Flares

The majority of stars maintain magnetic coronae of the type we see on the Sun; flares therefore abound on such stars. Their magnetic fields are generated by a dynamo at the interface between the radiative core and the convective envelope. They include main-sequence stars from spectral classes F to M, cool subgiants, and a large range of giants and supergiants in the cool half of the Hertzsprung-Russell diagram. Premain-sequence stars [T Tauri stars (TTS) and protostars] are very active coronal sources, and the same is true for some earlier-type, more massive young stars.

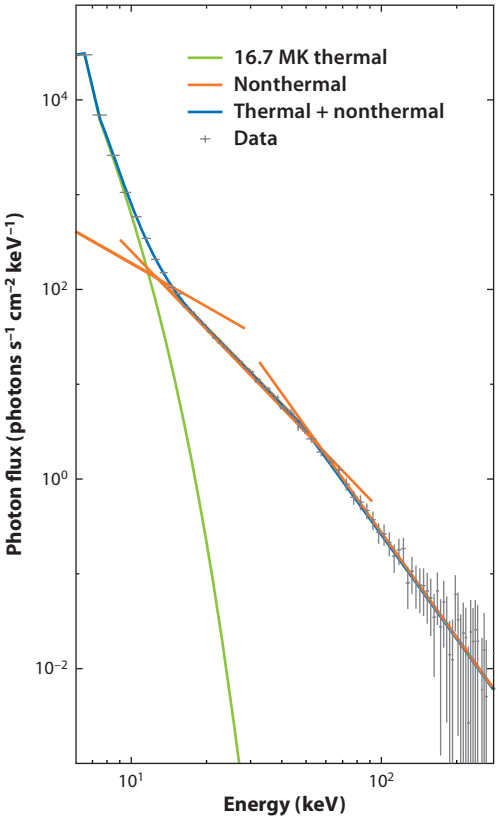

Figure 2

Bremsstrahlung emission during the impulsive phase of a solar flare observed by the *Ramaty High-Energy Solar Spectroscopic Imager* (RHESSI) satellite. At low energies, a thermal component (*green*) with a temperature of 16.7 MK has been fitted. At higher energies, a nonthermal component dominates. It is fitted (*orange*) by three power laws, yielding two breaks. The first, at 12 keV (if real), may be caused by the low-energy cutoff; the other break at 50 keV may have various origins as discussed in the text. The blue curve is the sum of the thermal and nonthermal components (from Grigis & Benz 2004).

Giant flares have been reported from class I and more evolved YSOs as soon as the circumstellar envelope becomes transparent to X-ray emission. Even substellar objects (brown dwarfs) are known to maintain solar-like magnetic activity. In this bigger picture, the Sun is a very inactive, spun-down G2 V star with a small surface magnetic filling factor, a faint chromosphere, and a rather modest X-ray and radio corona.

The basic working hypothesis applied to observations of stellar flares—and certainly the most important guide to understand their physical processes—is that of their being cousins of solar flares, evolving as a consequence of the same elementary physical mechanisms. Many stellar observations have clearly supported this picture. Most stellar flares show a similar time evolution, the initial (impulsive) phase producing the hottest plasma and the largest number of nonthermal radio-emitting particles. The flare plasma is much denser than the nonflaring coronal plasma, and the flare plasma cools characteristically on timescales of tens of minutes or hours as a consequence of radiative and conductive losses. Even a tentative classification into compact and two-ribbon (arcade) flares based on their X-ray light curves successfully uses the solar analogy (Pallavicini, Tagliaferri & Stella 1990).

Figure 3

Nonthermal hard X-ray and radio emissions of a solar flare overlaid on a soft X-ray image showing a flare loop (*green*). The average radio centroid positions observed with the Nançay Radioheliograph at 432 and 410.5 MHz are shown with a brown triangle and a blue square, respectively, at 327 MHz with a black dot, and at 236.6 MHz with a black star. Nonthermal *Ramaty High-Energy Solar Spectroscopic Imager* (RHESSI) observations at 18–25 keV (dominated by a coronal source) are in white contours, and at 25–50 keV (footpoint) in purple (Benz, Battaglia & Villmer 2010).

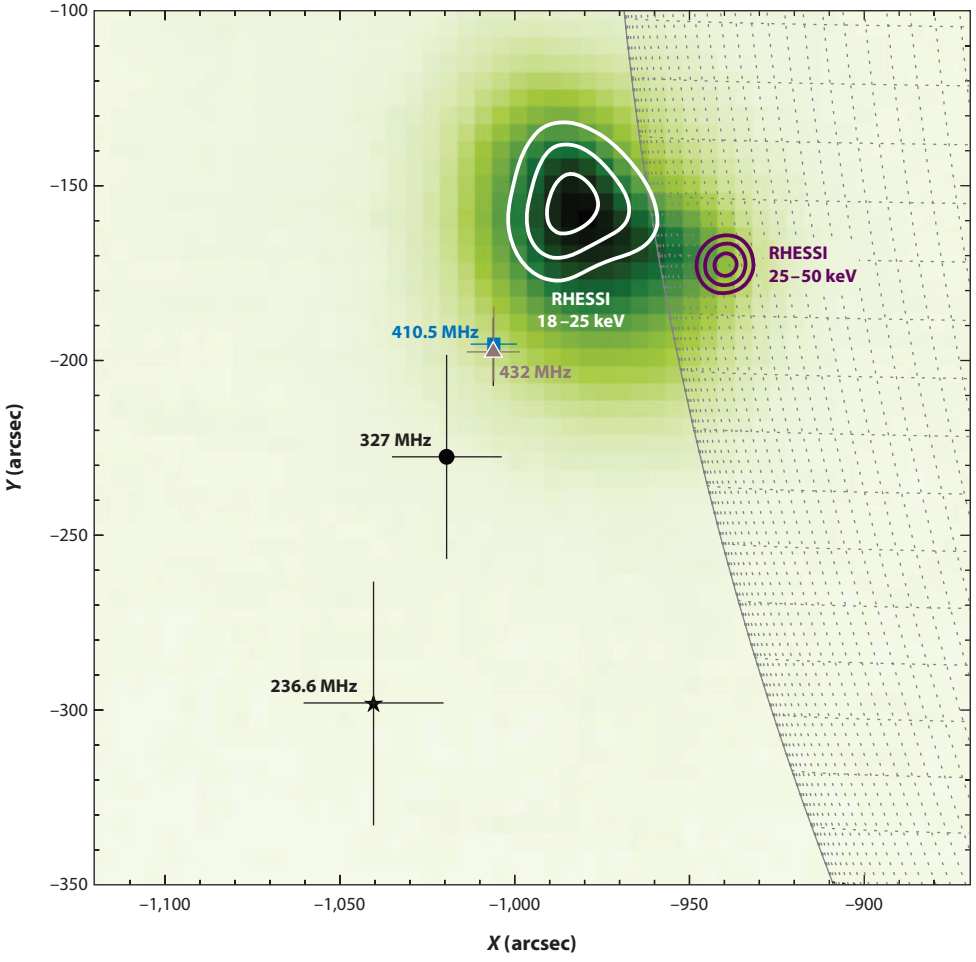

Nonetheless, stellar flares expand considerably the parameter range available to their solar analogs. On the one hand, observations of small flares in the crucial SXR band are rather limited by the available instrumental sensitivity and then reach down to energies of solar M-class flares for the nearest stars. Flares with an SXR luminosity of only $L_X \approx 2 \times 10^{26}$ erg s^{-1} and a total radiated SXR energy of 1.5×10^{28} erg were reported for Proxima Centauri (Güdel et al. 2002a). At the other extreme, however, flares emitting more than 10^{37} erg in X-rays, with peak luminosities around 10^{32}–10^{33} erg s^{-1}, have been observed (e.g., Kürster & Schmitt 1996, Skinner et al. 1997, Tsuboi et al. 1998, Favata & Schmitt 1999, Osten et al. 2007, Getman et al. 2008). Electron temperatures in such flares easily exceed 100 MK. Also timescales are sometimes extreme and cast doubt on the "solar analogy," as flares with decay times of order a day or several days are known from giants and subgiants (Graffagnino, Wonnacott & Schaeidt 1995; Ayres et al. 2001a; see also Kürster & Schmitt 1996), late-type main-sequence stars (Cully et al. 1994), and premain-sequence stars (Bower et al. 2003, Wolk et al. 2005, Getman et al. 2008). Even the flare rise phase may last a day or longer; solar "long-decay events" (Kahler 1977), albeit less extreme, may be the closest analogs to these stellar flares (Getman et al. 2008). Powerful radio flares have been observed as well; an extremely luminous flare on the FK Com-type giant HD 32918 lasted for 2–3 weeks, reaching a peak radio

luminosity of 6×10^{19} erg s^{-1} Hz^{-1} (Slee et al. 1987). For a broadband radio spectrum (with a spectral width of, say, ≈10 GHz), the integrated radio luminosity exceeds the total coronal X-ray luminosity of the nonflaring Sun by about three orders of magnitude! Similarly high luminosities may be seen from YSOs even at millimeter wavelengths, e.g., for the weak-lined T Tauri star GMR-A in Orion that reached a radio luminosity of $L_R \approx 4 \times 10^{19}$ erg s^{-1} Hz^{-1} at 86 GHz in a flaring episode lasting several weeks (Bower et al. 2003; Salter, Hogerheijde & Blake 2008).

In fact, extreme flaring behavior and features without solar analogy should be expected. Magnetically active stars reveal stronger surface magnetic fields, much higher total magnetic flux, higher magnetic filling factors, and therefore more volume for strong magnetic fields to interact but less space for the fields to diverge compared to the Sun. Global magnetic field configurations with strong dipole components have been suggested for fully convective or completely radiative stars, placing the regions of interest for magnetic energy release close to the poles or to regions high above the equator (Linsky, Drake & Bastian 1992; Benz, Conway & Güdel 1998; Donati et al. 2008). In close binary systems, magnetic fields anchored on the two stars may interact, and even close-in planets appear to drive magnetic activity in some systems (Shkolnik, Walker & Bohlender 2003). Premain-sequence stellar magnetic fields may reach out to the circumstellar disk, guiding accretion flows down onto the star. These fields are also subject to strong twist if the footpoints of the magnetic loops are not in coupled rotation. Giant flares and mass ejections may then be a consequence of star-disk magnetic field reconnection (Hayashi, Shibata & Matsumoto 1996; Montmerle et al. 2000).

A large range of the electromagnetic spectrum is available to stellar flare observations. The lack of spatially resolved observations is partially compensated by the availability of high-resolution spectroscopy, in particular, in the optical, UV, and SXR ranges. Radio observations especially by the Very Large Array (VLA) and the Arecibo 300-m dish have contributed much information about particle acceleration and nonthermal electron populations in closed magnetic fields (Bastian et al. 1990, Osten & Bastian 2006). Radio very long baseline interferometry (VLBI) constitutes the only direct way to spatially resolve flaring and nonflaring coronal features on stars other than the Sun, revealing global magnetic structure and polar magnetic fields (Benz, Conway & Güdel 1998; Mutel et al. 1998; Smith et al. 2003; Peterson et al. 2010). Optical and UV photometry and spectroscopy (using the *Hubble Space Telescope* and ground-based instruments) provide diagnostics tracing the reaction of lower atmospheric layers to flares (Hawley et al. 2003). They have also been used to derive flare occurrence rates. Tremendous progress has been made in recent years with SXR observations from the two large X-ray observatories, *XMM-Newton* (Jansen et al. 2001) and *Chandra* (Weisskopf et al. 2000), which have introduced high-resolution spectroscopy with resolving powers of a few hundred to about 1,000, following earlier spectroscopic studies in the EUV with the *Extreme Ultraviolet Explorer* (EUVE) (Bowyer, Drake & Vennes 2000). In contrast to solar investigations, stellar observations in the pivotal HXR (>10 keV) and the gamma-ray ranges must wait for more sensitive instrumentation, although some low-sensitivity records of 10–100 keV photons, perhaps related to a nonthermal flare component, are available (e.g., Osten et al. 2007). Timing studies of acceleration processes predominantly rely on radio observations, while U band/UV data provide good proxies for HXR emission.

3. OBSERVED PROPERTIES OF FLARES

3.1. General Characteristics

On September 1, 1859, the first solar flare was detected in enhanced continuum emission in optical wavelengths (white light) by the British astronomers R.C. Carrington and R. Hodgson.

The impulsive white-light brightening was associated with a magnetic disturbance and aurorae on Earth. Most solar and stellar flares show two principal phases. The initial impulsive phase is the period of the explosive release of energy, mostly in the form of accelerated particles and bulk mass motions, but also direct heating. Radiative signatures include optical/UV continuum radiation, nonthermal radio emission, HXRs, and gamma rays. The subsequent gradual phase is defined by cooling processes (although energy release may continue) following evaporative mass motions into the corona. It is best studied in SXRs, the EUV range (**Figure 1**), and in optical lines such as the Hα or other Balmer lines.

Optical photometric stellar flare observations have a long tradition, but it is the combination of photometry with line spectroscopy and the extension into the UV that has provided much new information on physical processes in flaring solar and stellar atmospheres (see Haisch, Strong & Rodono 1991). The optical and UV flare reveals itself in various lines, forming mostly in the chromosphere and transition region. In the Sun and in nearby stars, prominent coronal lines are observed in this wavelength domain as well.

Lines dominating during the (*a*) impulsive phase of flares include those of CII λ1335, CIII λ1176, CIV λ1548, SiII λ1265, SiIII λ1206, SiIV λ1394, OI λ1305, NV λ1239, and HeII λ1640 [see the emission line study by Hawley et al. (2003) for the M dwarf AD Leo]. Optical lines, predominantly revealing excessive flux in the (*b*) gradual flare phase, include the Balmer lines (Hα λ6563, Hβ λ4861, Hγ λ4341, and Hδ λ4102) and also HeI λ4871, HeI λ5876, and CaII λ8662. Lines from CaII H&K $\lambda\lambda$3934,3968 and MgII h&k $\lambda\lambda$2795,2802 contribute also predominantly to the gradual phase. Good, linear correlations exist between the time-integrated energies in Hγ, CaII, and the U band (Hawley & Pettersen 1991).

Flare-integrated energies in the Hγ line further correlate with integrated SXR energies (both being gradual-phase emissions; Butler, Rodono & Foing 1988). Many flares in active stars behave self-similarly by producing similar energy ratios between the above optical and UV lines (Hawley & Pettersen 1991). Apparently, the total flare energy scales with the surface area affected by the flare and the flare duration, with similar deposition rates for different flares. Solar white-light enhancements were observed only sporadically in extremely large solar flares, but have recently been discovered to be ubiquitous at lower levels accessible by space-based instruments. They receive interest as unique signatures of flare effects in the lowest part of the solar atmosphere. Solar white-light flare emission correlates with HXRs and is cospatial with HXR sources (Fletcher et al. 2007). This coincidence is surprising, as white light is generally believed to originate in the photosphere, but the HXR source is observed in the chromosphere (Christe & Krucker 2008).

HXRs are seen in the impulsive phase of a flare as bremsstrahlung, resulting from the bombardment of chromospheric and transition region layers by accelerated electrons. This prompt emission provides crucial timing information on the accelerator. Its spectrum, typically a power law or broken power law, can be inverted to infer the distribution of the nonthermal electron population (Brown 1971). Although HXR emission is easily observed from the Sun, its small flux prevents it from being routinely detected from stellar flares.

In SXR and the EUV range, flares produce thermal emission in the form of enhanced continuum radiation by optically thin bremsstrahlung from the hottest flare components and a variety of temperature sensitive lines. Most prominent are lines of Fe that populate much of this spectral domain. Line diagnostics based on Fe is unequalled because bright coronal Fe lines are available from many ionization stages (FeVIII–FeXXVI) forming at progressively higher temperatures across the entire coronal flare temperature range ($\lesssim 10^6 - 10^8$ K).

Flare radio emission comes predominantly in two variants, coherent and incoherent. Coherent radiation is excited by high-frequency waves, incoherent radiation by single electrons. Both radiations originate from nonthermal electron populations. A wide variety of coherent radio bursts,

often drifting in frequency as they evolve, provide diagnostics on the accelerator, the distribution of unstable electron populations, and density or magnetic field in the emission region (Benz 2002). Gyrosynchrotron radiation from mildly relativistic electrons (thus the prefix "gyro") injected into and trapped in closed magnetic fields is the dominant incoherent radio emission mechanism during flares. Its spectrum contains information on the magnetic field, the optical depth of the source, and the energy distribution of the injected electrons (Bastian, Benz & Gary 1998).

3.2. Flare Geometry

The energy of large flares is often assumed to be released at relatively high altitude in cusp-shaped magnetic fields. However, there are many reasons to question this assumption. The original idea of flares being caused by emerging flux would rather predict a low height (Gold & Hoyle 1960). There is ample evidence that tiny flares in the quiet Sun outside active regions (also known as nanoflares) occur at the heights of only a few thousand kilometers or even at chromospheric levels (Winebarger et al. 2002). Recent EUV observations by *Hinode* confirm earlier reports on continuous variability and flickering at the transition region (Brooks & Warren 2009, De Pontieu et al. 2009). Flaring may thus continuously affect transition region and chromospheric layers. Linsky & Wood (1994) (**Figure 4**) and Wood et al. (1996, and further references therein) found symmetrically broadened UV lines forming at 10^5 K in stellar transition regions, but broadening is absent in cooler (chromospheric) lines. This line broadening correlates with stellar activity, suggesting the presence of an increased rate of microflare-related "explosive events" in the transition region.

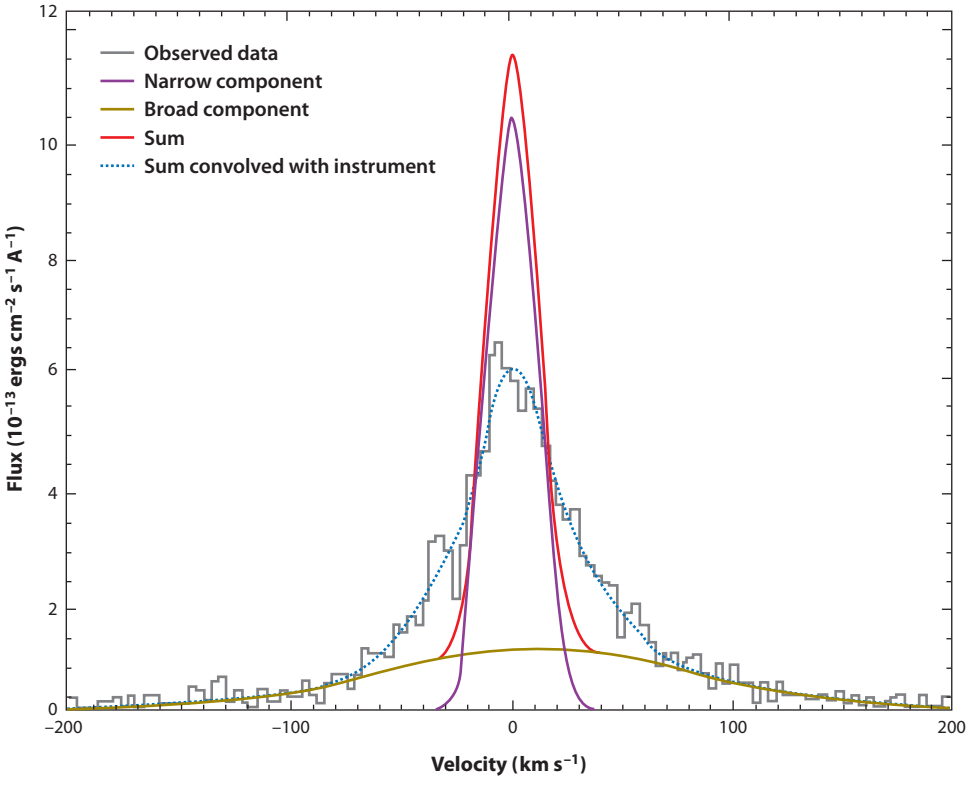

Figure 4

Broadened C IV line from the transition region of AU Mic. The histogram shows the observed spectrum. The solid lines show two Gaussian fits to the narrow (*purple*) and the broadened (*yellow*) components. The red line is the sum of both fits, and the dotted blue line gives the convolution of the sum with the instrumental profile (from Linsky & Wood 1994, reproduced by permission of the AAS).

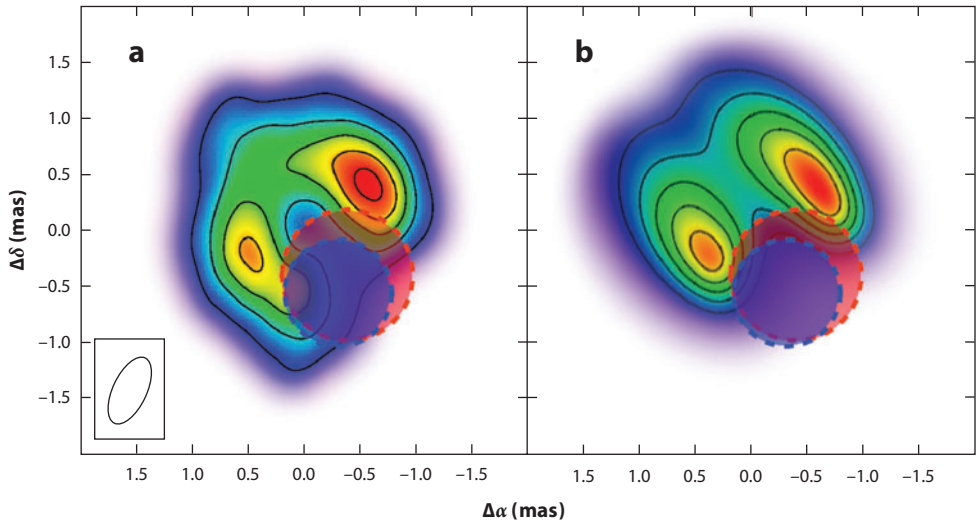

Figure 5

Radio contour maps of Algol in a flaring state, using very long baseline interferometry techniques at 8.4-GHz wavelength. The beam (indicating spatial resolution) is given in the lower left corner. (*a*) Observation; (*b*) a gyrosynchrotron model. The two circles (in *blue* and *red*) give the positions of the two stars during the observation (from Peterson et al. 2010; reprinted by permission from Macmillan Publishers Ltd).

In a new model of flare energy release, Fletcher & Hudson (2008) propose that the triggering reconnection takes place in the corona, but launches an Alfvén wave into the chromosphere where it accelerates particles.

In contrast, SXR images of large solar flares by the *Yohkoh* satellite suggest high-altitude reconnection (McKenzie & Hudson 1999). A hot (10^7 K) thermal source was seen within the cusp observed in CaXVII (Culhane et al. 2008). Coronal HXR sources, in addition to the footpoints in the chromosphere, are well known (Frost & Dennis 1971, Masuda et al. 1994; **Figure 3**). Krucker & Lin (2008) report an HXR component in 90% of the analyzed coronal sources. Coronal X-ray sources have a nonthermal component that is usually softer than the nonthermal component of the footpoints (Battaglia & Benz 2006). This is generally interpreted as the result of incomplete slow down of the radiating electrons being accelerated in the coronal source and escaping before thermalization (thin target). Petrosian, Donaghy & McTiernan (2002) propose that the coronal source is the acceleration site, partially containing the electrons during acceleration by scattering in wave turbulence.

An assessment of the magnetic geometry of flaring regions in late-type stars requires spatially resolved observations. Radio VLBI provides the only means to perform direct imaging of coronal sources. Large-scale radio-emitting coronae converging toward the magnetic poles have been reported with sizes up to several times the active star (Mutel et al. 1985; Benz, Conway & Güdel 1998). **Figure 5** shows the two footpoints of a flare loop of the K2IV star (Algol B, *larger red circle*) in the Algol binary system (distance 27 pc). Two bright sources are located near the poles of the active star. The modeled loop reaches a height of 2–4 stellar radii. Observations at other orbital phases indicate that the flare loops generally extend toward the expected circumstellar disk of the primary B star (Peterson et al. 2010). If the magnetic fields indeed attach to the expected disk of the primary, they will be subject to shearing motion that could trigger the flare seen in this observation.

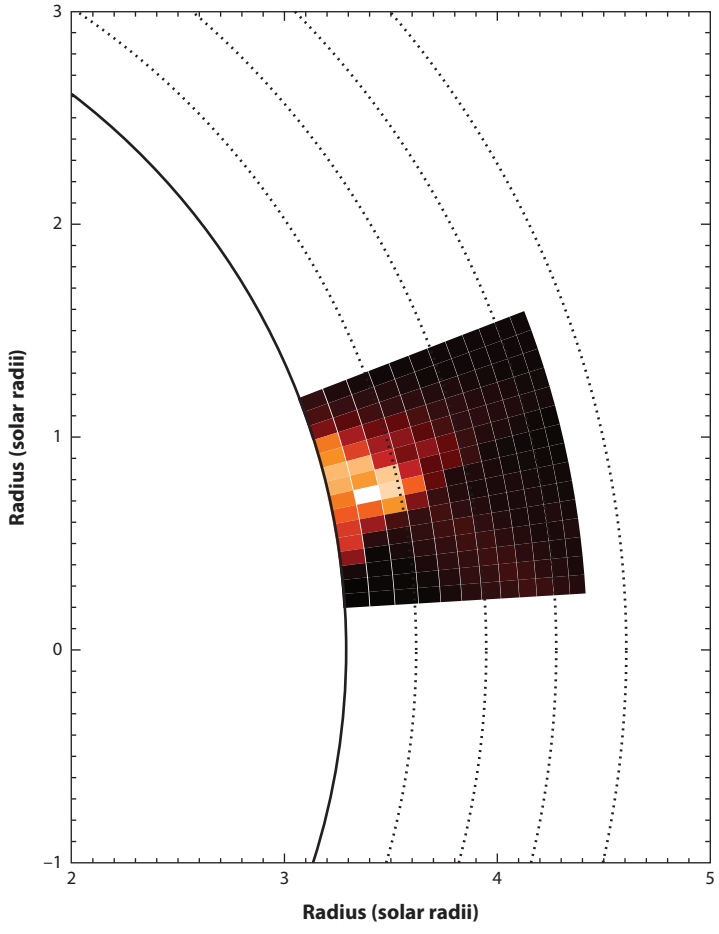

Figure 6

Limb view of an X-ray flare on Algol, reconstructed from an X-ray eclipse light curve. Axis labels are in units of the photospheric radius of the sun. Dashed circles give height in steps of 0.1 R_*. (From Schmitt, Ness & Franco 2003.)

New types of flaring geometries are possible in close binaries consisting of two magnetically active components. If the magnetic corona reaches to sufficiently high altitudes, intrabinary reconnection may be possible. Massi, Menton & Neidhöfer (2002) suggested, from periodic flare occurrences in the T Tauri binary V773 Tau, enhanced coronal interaction close to periastron passage in this eccentric binary. VLBI observations support this view by showing extended emission from both components elongated approximately toward each other, interpreted as extended structures similar to solar coronal helmet streamers (Massi et al. 2008).

Indirect evidence for stellar flare sizes comes from eclipsing systems if the companion star moves in front of an ongoing flare. The light curve can then be used to reconstruct the flaring geometry. In two X-ray cases (the contact binary VW Cep and Algol), near-polar flare structures with heights of no more than 0.5–1 R_* were inferred (Choi & Dotani 1998, Schmitt & Favata 1999). Another X-ray flare on Algol was located in the equatorial region, with a height of only 0.1 R_* (Schmitt, Ness & Franco 2003; **Figure 6**). Flares modulated by the rotation of the star itself may also reveal their sizes; Skinner et al. (1997) found evidence for a rotationally modulated flare decay, suggesting flaring source heights of only a few tenths of solar radii. We also mention a large body of reports on inferred flare sizes using model interpretations of the decaying light curves, summarized in Section 3.8.

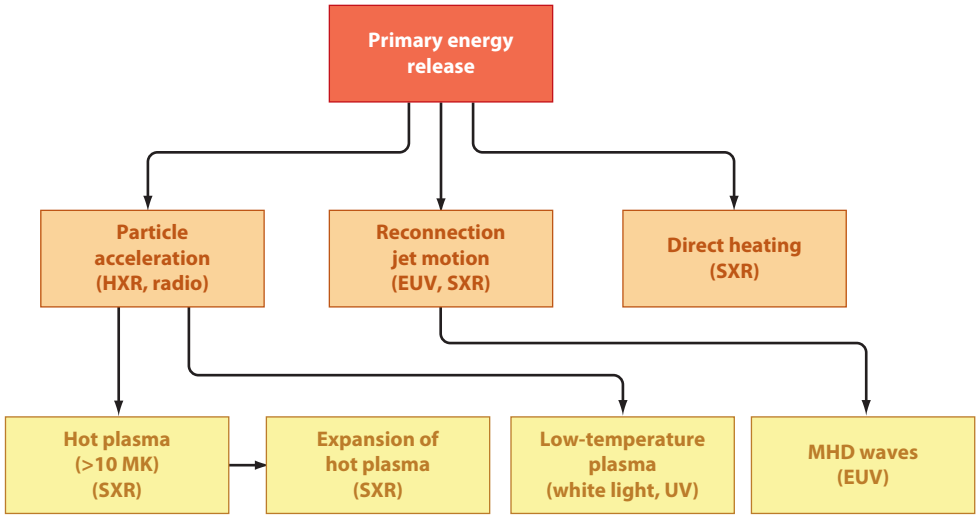

Figure 7

Schematic flow of energy from release (*top*) to primary products (*middle*) and secondary forms (*bottom*). Diagnostic radiations are indicated in parentheses. EUV, extreme ultraviolet; HXR, hard X-ray; SXR, soft X-ray; UV, ultraviolet.

3.3. Energy Channels

Magnetic energy exceeding the potential component can in principal be released. In terms of Faraday's equation, the free energy is contained in the $\nabla \times \mathbf{B}$ part of the field, causing an electric current. Initially, it can be released into three channels: heating, particle acceleration, and bulk motion (**Figure 7**). The partition into these primary products is parameter dependent. The way the energy is transformed into secondary forms also depends on the physical parameters and is discussed later.

In coronae of low-mass stars including the Sun, the thermal energy density is generally lower than the energy density of the magnetic field by more than an order of magnitude (low β plasma). In flare energy release regions the ratio β may be extremely low. The release of magnetic energy could thus heat the plasma to high temperatures. However, as discussed below, the thermal emission observed in SXRs and EUV wavelengths originates from much more material than initially present in the release region, indicating that direct heating is a minor recipient.

As the collision rate decreases with higher temperature, the energization of electrons and ions may result in particles with a non-Maxwellian (i.e., nonthermal) energy distribution; thus the process is termed acceleration. Magnetohydrodynamics (MHD) does not distinguish between heating and acceleration. The two particle distributions are evident in **Figure 2**, where X-ray emission of thermal electrons produces a characteristic spectrum at low photon energies, and higher energy electrons generate a distribution close to a power law. The energy distribution of the radiating electrons then must also follow a power law; hence they have a nonthermal distribution. For a power-law index larger than two (as usually inferred for electron energies), the power law must have a low-energy limit, where a cutoff or rollover keeps the integral in energy finite. The total energy is therefore dominated by the particles at low energy, thus by the cutoff energy.

The acceleration of ions is equally important. Flare-accelerated ions (mostly protons) impinge on the chromosphere and excite heavy ions, subsequently emitting nuclear lines observed for the Sun in the gamma-ray range. The spallation of ambient nuclei hit by an accelerated ion may produce a neutron. The neutron-proton capture line at 2.223 MeV (deuterium recombination) is well observed in large flares. From these lines the ion flux, spectrum, and total energy can be estimated. Ramaty et al. (1995) find that the energy contained in nonthermal protons above 1 MeV is similar within an order of magnitude to that in nonthermal electrons above 20 keV. Emslie et al.

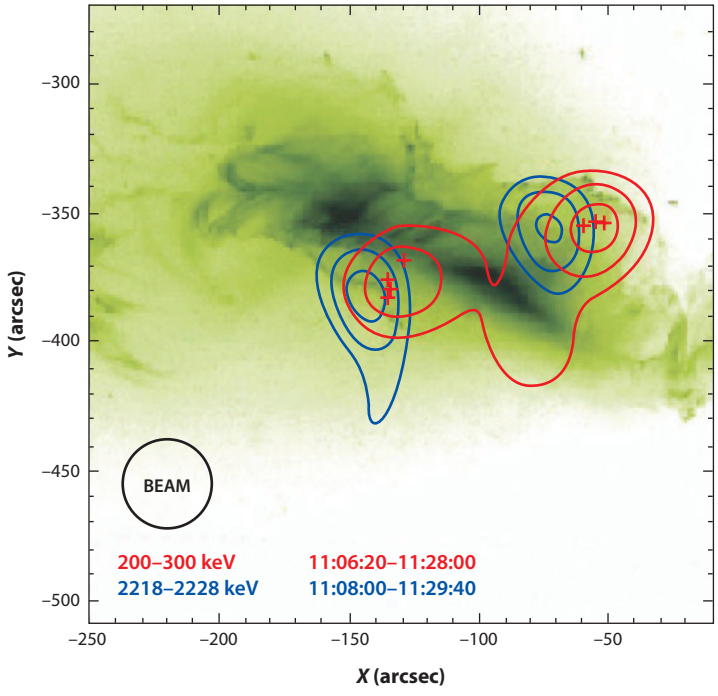

Figure 8

Footpoint emissions observed by *Ramaty High-Energy Solar Spectroscopic Imager* on October 28, 2003, in electron bremsstrahlung (*red*) and proton-produced deuterium recombination line (*blue*). The red crosses indicate the centroid positions at different times. The background image at 195 Å includes FeXXIV and CaXVII line emissions forming above 10 MK, observed by the *Transition Region and Coronal Explorer* satellite (Hurford et al. 2006, reproduced by permission of the AAS).

(2005) confirm this result. The footpoint sources of the proton-produced gamma-ray emission do not necessarily coincide with the nonthermal electron HXR (**Figure 8**). The displacement suggests differences in acceleration and/or propagation between nonthermal electrons and ions.

In the MHD view of reconnection, the energy is released by Ohmic heating in the current sheet and into the bulk motion of the reconnection jets (Priest & Forbes 2000). The latter is the other major primary product of reconnection. Innes et al. (1997, 2008) observed bipolar jets moving with the Alfvén velocity in chromospheric lines of solar flares. Reconnection jets in the corona and their energy are not well known. For a serendipitous case, Saint-Hilaire & Benz (2002) report an ejection decaying into turbulence within the corona (**Figure 9**). The energy of the ejection was found to be comparable to the energy in nonthermal electrons (after correcting the original work for the electron cutoff energy to 16 keV, corresponding to a photon cutoff at 10 keV). The magnetic field of the ejection is not considered in this estimate. If the reconnection jet reaches interplanetary space, a CME results. CMEs are discussed in Section 5.2.

3.4. Energy Dissipation

These results support the standard scenario in which the flare primarily accelerates high-energy particles. When they reach the chromosphere, they thermalize and heat the local plasma to temperatures of several 10^7 K in the solar corona, and up to $\approx 10^8$ K in strong stellar flares. As the flare X-ray radiation is optically thin, the flux can only increase by enlarging the emission measure, thus, for a constant volume, by additional material at high temperature. The additional thermal X-ray emission measure must consist of chromospheric material heated by precipitating flare particles or conduction.

This scenario has been suggested by Neupert (1968) to interpret the delay of thermal X-ray emission (or its proxies such as EUV emission or some chromospheric line emission, e.g.,

Figure 9

Transition Region and Coronal Explorer images near the solar limb (*white line*) at 195 Å (FeXII) with *Ramaty High-Energy Solar Spectroscopic Imager* half-power contours of two energy bands. The dotted blue contour corresponds to the 12–25 keV band, and the solid red contour to the 25–50 keV band. (*a*) The region of interest before the flare. (*b*) The rise of the hard X-rays (HXRs). (*c*) Between HXR and soft X-ray (SXR) peaks, showing the beginning of an ejection interpreted as a reconnection jet. (*d*) Between the SXR (3–12 keV) peak and the extreme UV peak (gradual phase). (*e*,*f*) The decay phase (Saint-Hilaire & Benz 2002).

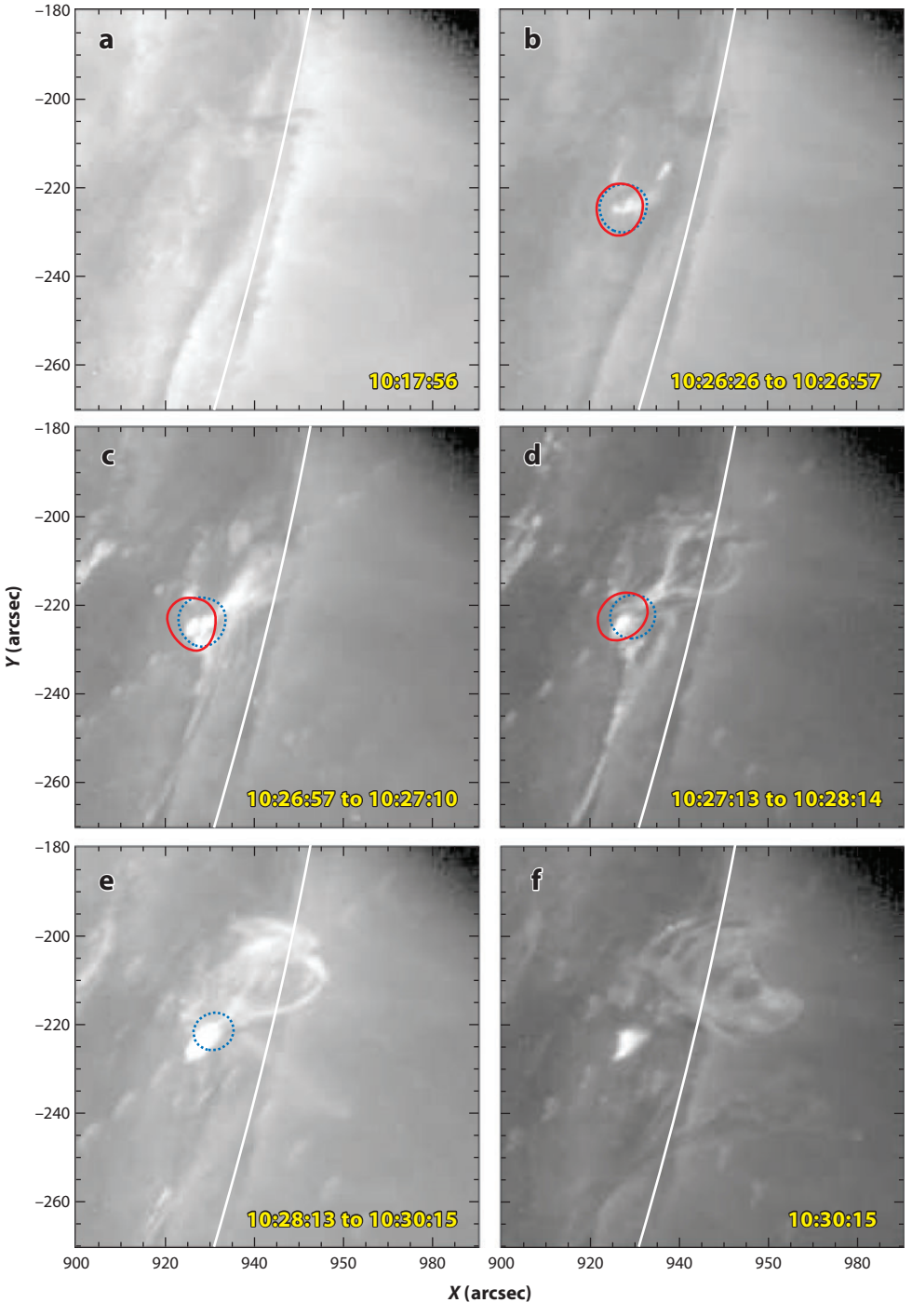

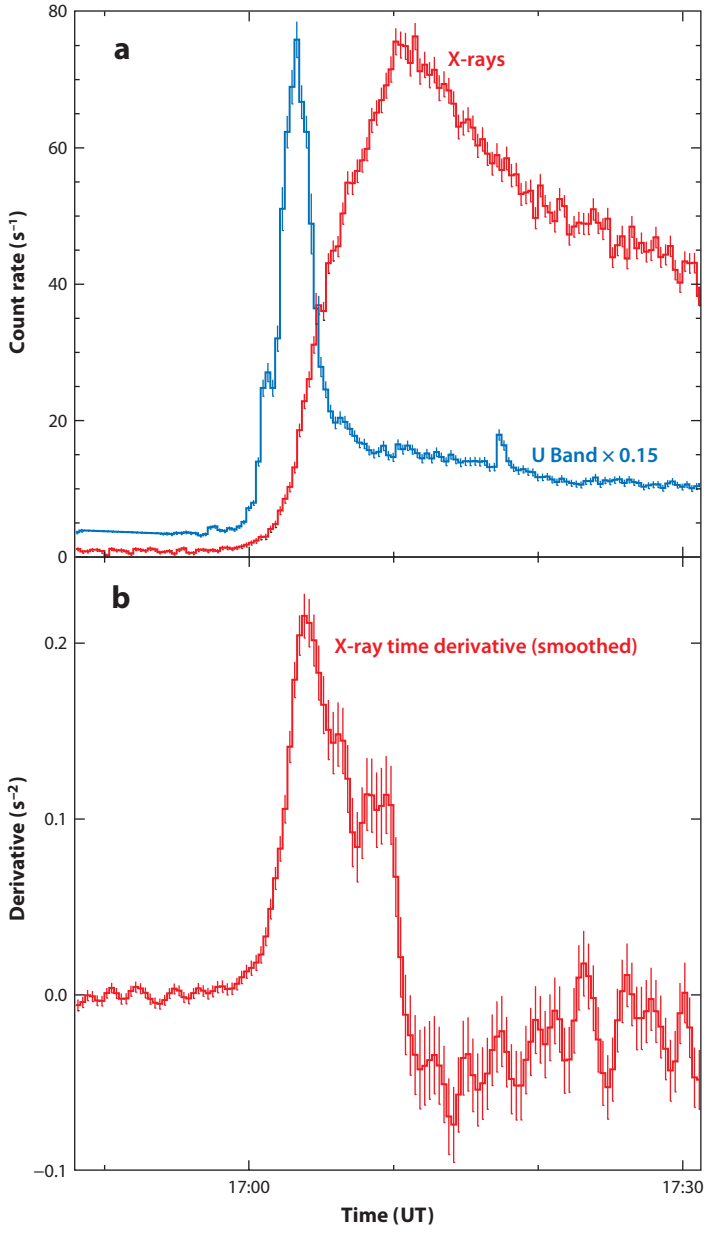

Figure 10

Neupert effect for a large flare on Proxima Centauri (main sequence, spectral type dM5.5e). Shown are (*a*) the soft X-ray (SXR) light curve, the U band light curve, and (*b*) the time derivative of the SXR light curve (after Güdel et al. 2002a).

from HeI or CaII) relative to nonthermal HXR and radio emission (or their proxies, such as U band continuum, white light, or many UV lines; see **Figure 10**). This "Neupert effect" is well observed in solar flares (e.g., Dennis & Zarro 1993) and is equally well known from stellar flares (Hawley et al. 1995, 2003; Güdel et al. 1996, 2002a; Osten et al. 2004, 2007; Wargelin et al. 2008; **Figure 10**).

The Neupert effect is not without exceptions, however. In four well-documented solar preflares, Battaglia et al. (2009) found thermal X-ray enhancements in the corona before any nonthermal

emission. They interpret it by a mostly thermal energy release (direct heating), followed by thermal conduction to the chromosphere, evaporation, and further heating. The temperature in the preflare is already at the level of the later flare phase. However, this thermal emission is more than an order of magnitude smaller than in the main phase. Overall, a Neupert effect is seen in only 80% of solar flares (Dennis & Zarro 1993) and is also often absent in stellar events (Smith et al. 2005). In extreme cases, very strong radio or X-ray flares show a complete absence of correlated behavior (Ayres et al. 2001b, Osten et al. 2005) or radio emission following the SXR flare in time (van den Oord et al. 1996, Osten et al. 2000). Interpretations are speculative and include eclipse effects and energy release in the chromosphere.

The energies in the nonthermal and thermal electron populations can be estimated from spectrally resolved, imaging solar X-ray observations. The ratio between nonthermal and thermal energies is about three on the average (Saint-Hilaire & Benz 2005, Emslie et al. 2005). Estimates are more difficult for stellar flares based on nonthermal gyrosynchrotron and SXR emission, but they indicate that the nonthermal energy is of the same order as, or exceeds, the radiative SXR output (Güdel et al. 2002b, Smith et al. 2005). A tentative interpretation of 10–100 keV emission as a nonthermal power-law tail during a large stellar flare also suggests order-of-magnitude agreement between the nonthermal energy and the total thermal (radiated plus conductive loss) energy (Osten et al. 2007).

If the energy in nonthermal electrons is larger than the thermal energy, where does the rest of the nonthermal energy go? Stellar studies indicate that similar fractions end up in the optical/UV and in the EUV/SXR ranges (Hawley et al. 2003). The breakdown of the optical versus UV energies varies between the impulsive phase, when UV lines are strong, and the gradual phase, when optical lines are strong. The ubiquitous blue continuum always dominates energetically the optical/UV emissions. The (total emitted) energy ratio between UV lines, optical lines, and the continuum is 0.07:0.02:1 during the impulsive phase and 0.05:0.18:1 in the gradual phase of M dwarf flares (Hawley et al. 2003). Observations by the *Solar Radiation and Climate Experiment* (SORCE) have seen an increase of the total solar irradiation during a flare for the first time (Woods, Kopp & Chamberlin 2006). At least half of the total irradiation enhancement resulted from UV radiation at wavelengths shorter than 200 nm. A large part of the remainder was emitted at UV wavelengths longer than 200 nm and in white light.

Models for M dwarf flares have been revealing. A photospheric/chromospheric/transition region model responding only to the X-ray/EUV radiation from an overlying corona is unable to reproduce all observed UV/optical lines in M dwarf flares, and also fails to explain the strong continuum. Although coronal flare X-rays irradiate the chromosphere and are reprocessed into optical and UV wavelengths (hydrogen recombination and UV lines) that are "backwarming" the underlying photosphere, an additional heating source, e.g., nonthermal electrons accelerated in the corona, is required at the top of the chromosphere (Hawley & Fisher 1992, Ding & Fang 2000). Part of the deposited electron energy will be radiated in UV and EUV lines to which the underlying chromosphere is transparent, thus leading to further photospheric heating. The resulting continuum should therefore be due to blackbody radiation ("UV/EUV backwarming" driven by nonthermal electron heating of the chromosphere), consistent with solar observations (Hawley & Fisher 1992; blackbody temperatures typically being at 9,000 K). The optical continuum should therefore temporally correlate with HXRs, as indeed observed in the Sun.

3.5. Statistical Correlations

As suggested in the section above, the hot plasma that emits thermal X-rays does not contain the total energy released in the flare, but it is a good tracer of the energy and can be conveniently

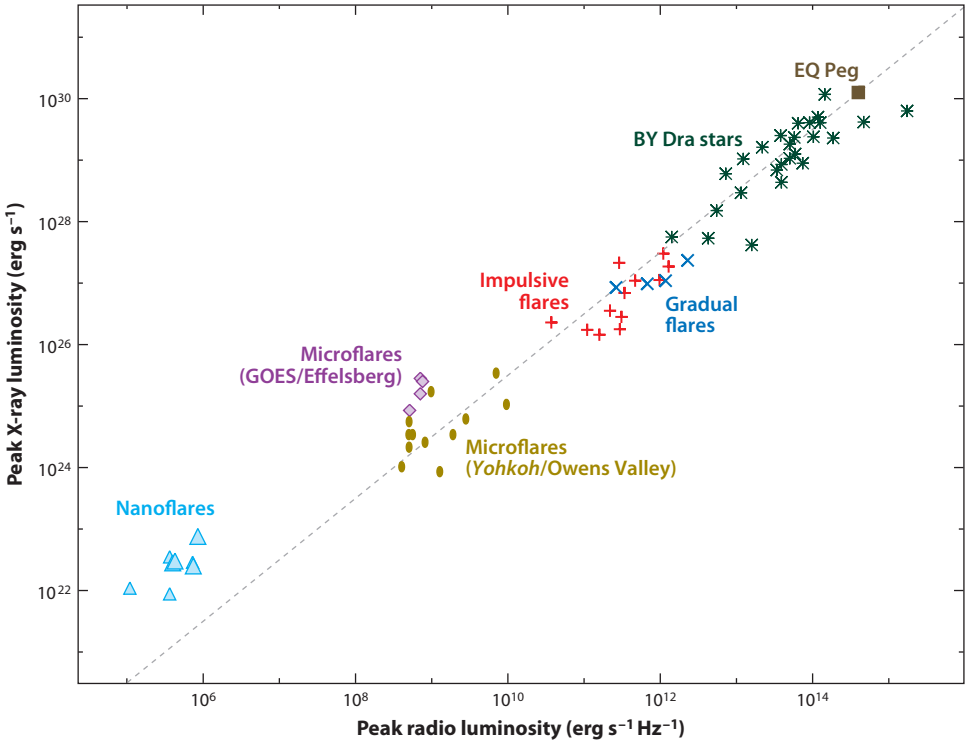

Figure 11

Comparison of the soft X-ray and centimeter radio luminosities (peak values for flares) from nanoflares in the quiet Sun, over microflares and regular solar flares, quiescent dMe, dKe, and BY Dra stars (Güdel & Benz 1993; *asterisks*), to a long duration flare on the dMe star EQ Peg (*brown square;* Kundu et al. 1988). The dashed line is a fitting curve with slope 1 given by Equation 1 (Krucker & Benz 2000).

measured also in stars. The energy conversion to X-ray-emitting plasma is lossy. Nevertheless, a tight correlation between SXRs (comprising most of the thermal emission) and the peak HXR flux at 35 keV, in the 20–40 keV band (nonthermal emission), was reported for solar flares by Battaglia, Grigis & Benz (2005) and extended to stars by Isola et al. (2007).

Gyrosynchrotron radio emission at centimeter waves is emitted by mildly relativistic electrons in the high-energy tail of the nonthermal distribution. The peak fluxes of HXRs (>30 keV) and centimeter waves (at 17 GHz) correlate linearly in solar flares (Kosugi, Dennis & Kai 1988). Therefore, the radio emission is a convenient proxy for nonthermal electrons accelerated in stellar flares.

The correlation of gyrosynchrotron emission with thermal X-rays is shown in **Figure 11**. The flares range from the smallest events in the quiet-Sun network over regular flares in active regions to a very large stellar flare. The figure also includes apparently quiescent emission of main-sequence dMe and dKe stars, and active binaries. The relation is linear in the high-energy part, where

$$L_X/L_R \approx 10^{15.5\pm0.5}\,[\mathrm{Hz}] \qquad (1)$$

(L_X is again the SXR luminosity in units of ergs per second, and L_R is the gyrosynchrotron radio luminosity in units of ergs per second per hertz; Benz & Güdel 1994). The similarity of the ratio of thermal to nonthermal emission, L_X/L_R, over many orders of magnitude in luminosity is surprising. The proportionality suggests that all flares follow the same basic scenario of electron acceleration, transport, and chromospheric heating. The only substantial deviation is at the low-energy end. The extremely small flares in quiet solar regions are radio poor, indicating a reduced amount of electron acceleration and/or magnetic field strength. The nearly constant L_X/L_R ratio in flare-like energy releases can be used to test the nature of a phenomenon and the mechanism

of the associated radio emission; it further suggests that much of the apparently nonflaring radio and X-ray radiation from magnetically active stars is in fact due to flares, a suggestion for which further support is summarized below. The correlation breaks down for flares that do not reflect the standard solar behavior (e.g., showing absence of the Neupert effect, see above). It is also not applicable when the radio emission is dominated by radiation other than gyrosynchrotron (e.g., thermal emission or coherent radiation). Finally, care should be taken when interpreting radio bursts, in particular from very low-mass stars and brown dwarfs. Their radio emission is often dominated by some coherent radiation mechanisms and does not follow the standard radio-X-ray behavior (e.g., Kundu et al. 1988 for M dwarfs, Berger 2006 for brown dwarfs, and Hallinan et al. 2008 for periodic radio pulses in low-mass objects interpreted as highly directive maser emission).

Observations of magnetically active stars also revealed a linear correlation between the time-averaged power from optical flares and the low-level, "quiescent" X-ray luminosity. This correlation could be explained if the mechanism that produces the optical flares also heats the plasma to X-ray emitting temperatures (Doyle & Butler 1985, Skumanich 1985, Whitehouse 1985). In the solar context, the monthly average SXR luminosity scales in detail and linearly with the rate of detected Hα flares throughout the solar cycle (Pearce et al. 1992). Analogously, the quiescent X-ray luminosity of magnetically active stars correlates approximately linearly with the rate of X-ray flares (above some lower energy threshold) (Audard et al. 2000; see also Stelzer et al. 2007 for T Tauri stars); this is expected if all X-ray emission originates from a distribution of flares (see Section 5.1). Similar trends have also been noted for U band flares and the quiescent U band luminosity of active stars (Lacy, Moffett & Evans 1976).

Further, the ratio between energy losses in coronal X-rays and in the chromospheric MgII lines is the same in flares and in quiescence (Haisch et al. 1990). This applies also for UV-filter observations (Mitra-Kraev et al. 2005). Finally, a tight correlation between L_X and Hγ luminosity of active stars agrees between flares and quiescence (Mathioudakis & Doyle 1990). These observations point to an intimate relationship between flares and the overall emission from the hot outer atmospheres of stars.

3.6. Flare Amplitude Distributions

Based on the statistical correlations above, the thermal SXR flux may be assumed to be on average proportional to the total flare energy released. As accelerated particles comprise a significant fraction of the flare energy, the nonthermal X-ray flux integrated in time and energy may also be a good proxy. Both tracers have their deficiencies. The thermal SXR emission at any instant yields the emission measure. With a measured temperature assumed to be uniform and an estimated volume, the thermal energy of the plasma can be calculated. The SXR peak flux yields only a lower limit, missing the radiated energy before the peak and in other wavelengths. Alternatively, the SXR light curve can be integrated in time and energy to arrive at the total energy that is radiated by the coronal part of a flare. This energy does not include losses by thermal conduction. The integrated nonthermal HXR flux requires an assumption on the low-energy cutoff (Section 3.3) and lacks the energy of bulk motion in the reconnection jets and in waves. Thus, the total energy of flares is not well constrained.

Nevertheless, flares reveal a frequency distribution, $f(E)$, that can be approximated by a power law in energy, as estimated from electron fluxes, thermal energy content or radiated power. This shape of the distribution is a remarkable property by itself. In particular, the energy of flares, E, is distributed as

$$\frac{df(E)}{dE} \approx f_0 E^{-\alpha}, \tag{2}$$

where $df(E)$ is the number of flares per time with energy between E and $E + dE$. The total energy in nonthermal electrons has been found to have a power-law distribution over more than three orders of magnitude in the seminal paper by Crosby, Aschwanden & Dennis (1993). The range is limited by instrumental sensitivity on the low-energy side and the small number of large flares in the limited observing time at the high-energy end.

The amplitude distribution in the form of a power law means that the flare process is scale invariant within the observed range. There are two competing interpretations of this behavior. (*a*) Rosner & Vaiana (1978) proposed a scenario in which magnetic energy in an active region builds up exponentially in time, but is released after a random duration. (*b*) A power-law distribution can also result if the flare consists of an "avalanche" of a large and random number of small events. Lu & Hamilton (1991) proposed such a statistical flare model based on the idea of a self-organized system in a critical state (sand pile model). However, Battaglia, Grigis & Benz (2005) found that large flares in nonthermal X-rays have a harder (flatter) spectrum and, thus, cannot simply be composed of many small flares.

For the total energy released by flares, the distribution $f(E)$ has to be multiplied by the energy and integrated. Depending on the power-law index being smaller or larger than two, the large or small flares dominate, respectively (Hudson 1991). For solar flares in active regions, an index smaller than two has been reported by several researchers (e.g., Crosby, Aschwanden & Dennis 1993). Thus, few large flares appear to deposit more energy into active regions than the many small ones. This conclusion has recently become disputed again, as all previous researchers have assumed a fixed electron low-energy cutoff near 25 keV. However, Lin, Feffer & Schwartz (2001) point out that most of the electrons' energy in small flares is in particles at lower energy. Taking advantage of RHESSI's spectral resolution, Hannah et al. (2008) have measured the cutoff energy or its upper limit. They find two orders of magnitude more energy (median values) in small flares than with a cutoff fixed at 25 keV. Their frequency distribution is not a power law. The last word on the frequency distribution of solar flare energy is still out.

What is unclear for large solar flares that appear isolated in time even in full-Sun observations is even more disputed for small flares (sometimes called nanoflares) in quiet regions. The power-law index derived by different methods ranges from 1.80 (Aschwanden et al. 2000) to 2.59 (Krucker & Benz 1998). It is converging toward 2.0 (Benz & Krucker 2002), but there is no agreement as nanoflares overlap in time and space, and the smallest events are elusive. Winebarger et al. (2002) report an index of 2.9 ± 0.1 for explosive events observed in the transition region. An index of 2 would mean that all decades in flare energy release an equal amount of energy. The discussion is relevant to the question whether the flare energy input from unresolved small events provides the energy input for coronal heating, discussed in Section 5.1 below.

The situation is again different for magnetically active stars. The limited sensitivity has restricted flare statistics essentially to magnetically active stars, revealing a high cadence of luminous flares. Recent statistical studies are based on the total radiative flare energy in SXRs or EUV wavelengths. Although smaller flares have been recorded (Section 2.2), statistical studies start typically at 10^{31} erg. Recent studies find α in the range of 2–2.5 for G–M dwarfs (Audard et al. 2000, Kashyap et al. 2002, Güdel et al. 2003) and for T Tauri stars (Stelzer et al. 2007). Therefore, it appears that in magnetically active stars, the bulk of the energy release by flares comes from the large number of small events that may not be resolved individually in the observed light curves (see Section 5.1 below for further discussion).

Flare energy distributions of "flare stars" were studied already a long time ago in the optical and, in particular, in the U band, for which Lacy, Moffett & Evans (1976) and Gershberg & Shakhovskaia (1983) concluded that α is mostly in the range 1.4–2.0; only a small fraction (of

order 10^{-4} L_{bol}, and a few percent of L_U) of the luminosity can be due to the observed flares. In the UV domain, Saar & Bookbinder (1998) monitored the transition-region lines of SiIV and CIV (forming at $\approx 10^5$ K) in two active stars near the zero-age main sequence and found rather hard distributions with $\alpha = 1.0 \pm 0.1$ and 1.5 ± 0.1, respectively, for the two targets. These distributions may not be directly relevant for the coronal heating problem due to possible nonlinearities between optical flare power and the heating power in the corona.

3.7. Chemical Abundances

It is well known that elements having a low first ionization potential (FIP) are overabundant by a factor of 3–4 in the solar corona. Stellar EUV and X-ray spectroscopy has uncovered a number of anomalies of stellar coronal plasma composition compared to the solar FIP effect. In brief, magnetically active stars reveal coronal plasma that is systematically deficient in low-FIP elements compared to high-FIP elements (a trend opposite to the solar composition, therefore coined "the inverse FIP effect"; Brinkman et al. 2001). Overall, most elemental abundances appear to be low. In contrast, inactive stars may show enhanced low-FIP element abundances in analogy to the solar FIP effect (Laming, Drake & Widing 1996; Telleschi et al. 2005). There is a clear trend from IFIP-biased coronae to FIP-biased coronae with decreasing stellar activity (Telleschi et al. 2005). The enhanced Ne/Fe abundance ratios observed in active coronae could be due to (continuously occurring) anomalous flares such as Ne-rich flares seen on the Sun (Schmelz 1993) and in stars (Wargelin et al. 2008).

It has long been known that the "metallicity" of flares on magnetically active stars tends to increase compared to their nonflaring coronae (e.g., Ottmann & Schmitt 1996). Interestingly, the metallicity seems to be bounded by the solar photospheric metallicity, suggesting that fresh material was brought up into the corona as a consequence of evaporation (assuming that the stellar photosphere is composed of a similar mix as the solar photosphere, which is not generally true, however). Spectroscopic studies showed for some stellar flares that it is predominantly the low-FIP elements that become enhanced during flares (Güdel et al. 1999; Osten et al. 2000; Audard, Güdel & Mewe 2001), again suggesting that the coronal IFIP composition is diluted by evaporating material. These trends were systematically studied by Nordon & Behar (2008), who found that flares on stars with FIP-biased coronae develop a "relative" IFIP composition and vice versa. Apart from confirming the scenario of evaporation of unfractionated photospheric material, this finding suggests that the observed coronal composition anomalies are genuine and not only reflecting the (often poorly known) photospheric composition.

The FIP trends discussed above thus pose a problem for theories of flare-induced coronal heating. Although large flares "reset" the coronal composition (i.e., adding low-FIP material to an IFIP corona), small flares would need to operate differently to generate the strong IFIP fractionation seen in magnetically active stars outside obvious flares.

3.8. Cooling in the Gradual Flare Phase

Flares cool mostly by radiation and conduction. Radiative cooling dominates in the late phase of the flare, the gradual phase, when SXR emission becomes the outstanding diagnostic of the flaring region. A comprehensive characterization of the cooling phase and the complex magnetic structure seen in SXRs and the EUV wavelengths in this phase is not a focus here but reviewed by Favata & Micela (2003) and Güdel (2004) for stellar observations. Here, we briefly summarize main issues from the recent literature.

The gradual flare phase provides diagnostics for the structure of magnetic loops, continued heating, and basic physical parameters such as densities and pressures. These diagnostic means are irreplaceable for stellar flare studies in which spatially resolved observations are the exception. A number of light curve diagnostics are available based on the fundamental cooling processes of radiation (proceeding in proportion to the square of the electron density, n_e) and conduction (related to temperature). In the case of collisionally dominated conduction (termed Spitzer or classical conductivity) the loss rate is proportional to $T^{7/2}/L^2$, where L is the characteristic length connecting the hot coronal source with the cool chromosphere/photosphere. We note, however, that even in solar preflares, conduction was found to be saturated and, thus, nonclassical (Battaglia, Fletcher & Benz 2009).

If the dominant cooling process were known, the decay timescale of the light curve could be used to infer n_e (and therefore, from observations of the emission measure, the flaring volume) or L. More realistic models include, among others, the following:

- Combined radiative and conductive cooling related to observations of temperature and emission measure decay times (van den Oord, Mewe & Brinkman 1988),
- Quasi-static cooling loops that evolve through a sequence of static solutions in which continued heating balances the total energy losses (van den Oord & Mewe 1989),
- Consideration of a scaling law for the thermodynamic decay of the hot plasma, depending on the loop length L and the peak temperature, compared with the observed decay of temperature and emission measure to infer the amount of continued heating during the decay (Reale et al. 1997),
- An analytic "two-ribbon" flare model in which open magnetic field lines reconnect in successively higher layers; here, the light curve development in fact depends on the heating rate during the entire flare evolution, which in turn depends on the energy available in nonpotential fields (Kopp & Poletto 1984),
- Scaling laws for the magnetic field strength, the peak temperature, the preflare density, and the characteristic flaring loop length, based on MHD X-point reconnection calculations (Shibata & Yokoyama 1999, 2002), and
- To these, we should add the many numerical simulation techniques that have been used to follow the evolution of the thermal flare plasma from the initial energy release through evaporation and late cooling (e.g., Peres et al. 1982; Mariska, Emslie & Li 1989; Cheng & Pallavicini 1991).

These diagnostic models are more comprehensively described in Güdel (2004). Among the key results figure the following:

- Flaring plasma requires electron densities typically in the range of 10^{10}–10^{12} erg cm^{-3}.
- Flaring loop or arcade sizes are moderate even for strong stellar flares; characteristic sizes are a few tenths of a stellar radius. Exceptions may exist for very energetic, slowly decaying flares for which large volumes or large loop lengths may be required.
- Continued heating input is often required during the flare decay phase.

The relative compactness of many flaring regions on stars comes together with similar estimates for the nonflaring thermal, X-ray-emitting coronae. However, such moderate sizes contrast with some very extended flaring structures seen at radio wavelengths using VLBI (e.g., Benz, Conway & Güdel 1998; Peterson et al. 2010). The most obvious explanation for the apparent discrepancy is that the SXRs originate in dense, compact postflare loops (because the emissivity scales with n_e^2). In contrast, energetic electrons survive the longest in low-density, extended magnetic structures where they lose relatively more energy by the gyrosynchrotron process.

RECONNECTION

To define reconnection, we consider two adjacent magnetic field lines that are locally oppositely directed (**Figure 12**). Let us concentrate on the segments from A to B on one of the lines and from D to C on the other one. Reconnection then changes the linking so that the new lines connect A to C and D to B, respectively. The magnetic field in between disappears and is said to have annihilated. For reconnection to occur, the magnetic field must diffuse through the region between the initial location of the lines. This process is described by resistive MHD.

The scenario of diffusing magnetic field lines is fully equivalent to the description by electric currents. Ampère's law requires that a current flows between the oppositely polarized field lines. Reconnection thus requires that the current is dissipated.

4. BASIC PROCESSES

4.1. Magnetic Reconnection and its Configurations

In a stellar atmosphere where closed loops of magnetic fields emerge stochastically, magnetic reconnection is a necessary process to limit the energy density and the geometric complexity of the magnetic field (see the sidebar, Reconnection). Reconnection reconfigures the magnetic configuration to a lower energy state, releasing energy to the environment. Although reconnecting magnetic field lines is not the only way to release magnetic energy, reconnection plays an important role in plasmas with low resistivity. In such plasma, magnetic energy can build up between oppositely directed field lines, forming a thin current sheet (**Figure 12**). The current density increases the thinner the sheet becomes, until reconnection impulsively releases the stored energy.

Even in a tenuous plasma like a stellar corona, MHD describes well the quasi-steady build up of a configuration that will reconnect. If collisions prevail, resistive MHD predicts that about half of the magnetic energy is dissipated by Ohmic resistance. The rest resides in the bulk motion of the newly formed magnetic loops that snap back into a force-free position, thus forming reconnection jets (Priest & Forbes 2000). In a dilute plasma, normal resistive MHD predicts a reconnection timescale orders of magnitude longer than observed in flares. The discrepancy may be explained by anomalous resistivity enhanced by electromagnetic turbulence that is driven by some current instability. It effectively increases the electron collision rate.

Criticism of reconnection controlled by anomalous resistivity has come from the Earth's magnetotail, where the wave level observed is a hundred times too small (Bale, Moser & Phan 2002).

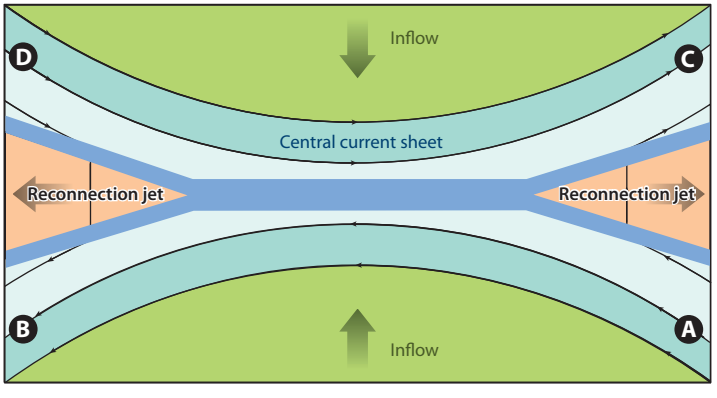

Figure 12
Schematic view of basic reconnection in two dimensions. Labels refer to discussion in the text.

However, evidence for thermal electrons trapped by electric fields providing effective resistivity has been reported by Egedal et al. (2008). As the plasma parameters in the magnetotail are orders of magnitude different from the flare energy release sites and the energies involved differ greatly, the value of the analogy is limited.

An alternative is collisionless reconnection. In the absence of collisions, the reconnecting current sheet shrinks to the dimensions of the proton inertial length (c/ω_{pi}, where ω_{pi} is the ion plasma frequency) or, if larger, the ion gyroradius. The mean free path of ions in atmospheric plasmas is generally much larger than this scale. The ions thus are collisionless in the relevant crossing time and decouple from the magnetic field. The behavior of ions and electrons diverges and the MHD approximations are no longer valid. The reconnection process is then called collisionless. In situ observations of collisionless reconnection in the Earth's magnetotail demonstrate that this process rapidly releases energy (Øieroset et al. 2001). It is not clear how these results apply to the orders-of-magnitude denser solar and stellar atmospheres, but a similar behavior has been noted in lab plasmas that have higher densities (Zweibel & Yamada 2009). The transition from slow collisional reconnection before the flare to collisionless reconnection in the main flare phase has been modeled by Cassak, Drake & Shay (2006). The change increases the reconnection rate by many orders of magnitude in a very short time. This property may explain the impulsiveness of reconnection in flares. Evidence for the equality of proton inertial length and current sheet thickness in solar and stellar flares has been presented by Cassak, Drake & Shay (2008).

Locally opposite magnetic fields have been proposed in many large-scale configurations (**Figure 13**). Differences exist in the cause of reconnection and the way the reconnection process is driven. Most diagrams involve basically only two dimensions. Theory shows that reconnection in 3D has even more features than the standard 2D pictures. In particular, we note that it is not necessary that fields are oppositely directed. It is sufficient for reconnection that there is some shear.

In the most popular solar flare scenario, the top of a loop expands and rises (**Figure 13*a***). This motion drags along magnetic flux that is constricted below the driving plasmoid. Reconnection occurs and reduces the stress on the plasmoid. Opposite field lines approach each other and reconnect. Hot plasma forms a cusp below the reconnection site. Cusp-shaped thermal X-ray sources have been observed (**Figure 14**), and loops shrinking in the lower part have been reported by Reeves et al. (2008). The final shape is termed helmet streamer.

An axisymmetric, global cusp-shaped magnetic field structure from pole to pole has been proposed for chemically peculiar B and A stars (Linsky, Drake & Bastian 1992). This model features global (near-dipolar) field lines drawn into an equatorial current sheet by a wind, forming a cusp-shaped configuration (**Figure 13*a***) in the equatorial plane. Particles would thus be accelerated in the equatorial current sheet and be trapped in lower, van Allen belt-like toroidal structures. Similar models were proposed for large halo structures in RS CVn-type binaries (Morris, Mutel & Su 1990) or in massive premain-sequence stars (André et al. 1988). Systematics in radio polarization provide evidence for such global magnetic structure.

Colliding loops (**Figure 13*b***) must be expected when new magnetic flux emerges through the photosphere. The best evidence is from nonthermal X-ray flares or centimeter radio observations showing four footpoints, where energetic particles precipitate (Aschwanden et al. 1999).

Interchange reconnection (Heyvaerts, Priest & Rust 1977; Fisk 1996; see **Figure 13*c***) of a field line that is open to interplanetary space and a closed loop has been proposed to interpret the footpoint motions of solar wind field lines and the escape of electron beams in flares. Reconnection occurs when emerging flux pushes against open field lines or the open field line is dragged over the closed loop by the solar wind rotating more slowly than the closed loop.

Magnetic arcades are frequently observed in the solar atmosphere. They extend above the neutral line of the vertical photospheric field. When the footpoints move at different speeds, the

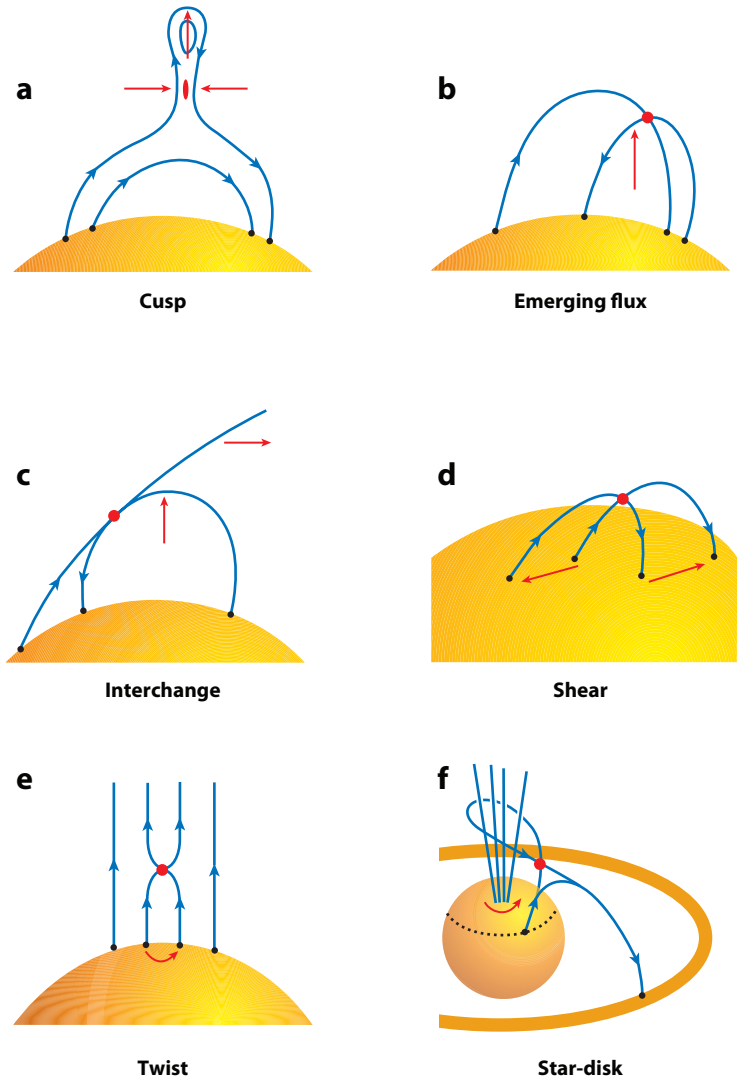

Figure 13

Various large-scale geometries leading to reconnection. The driving forces are marked by arrows and reconnection sites by red dots. Large erupting flares are often surmised to result from a magnetic cusp (*a*). The emerging flux scenario (*b*) may apply to smaller events in the low corona. Interchange reconnection (*c*) is associated with flares at high altitude, leading to interplanerary particle events. Magnetic shear (*d*) may be the cause of two-ribbon flares, where the footpoints form two parallel strands. Reconnection of twists (*e*) releases energy in loops. In the star-disk interaction (*f*), reconnection releases energy build-up by stellar rotation.

arcade is sheared and magnetic energy builds up in the corona (**Figure 13*d***). This energy may lead to a large flare characterized by two bright ribbons in the chromospheric Hα line or EUV emissions from the transition region.

Braiding field lines by footpoint rotation have been proposed by Parker (1988) to cause oppositely polarized components in field lines and tiny reconnections (nanoflares) in stationary loops (**Figure 13*e***).

Young low-mass stars are strongly magnetized and interact with circumstellar disks through a corotating corona, usually envisioned in terms of a dipolar magnetosphere. Marginal evidence for magnetospheres reaching out to the inner border of circumstellar disks comes from radio VLBI observations, in particular of the southern component of T Tau Sb. A source diameter of 0.07 AU or 15 R_* was derived, and radio bursts were detected within this source (Smith et al. 2003). **Figure 13*f*** shows a field line seen from an observer orbiting with the disk. If the star rotates faster,

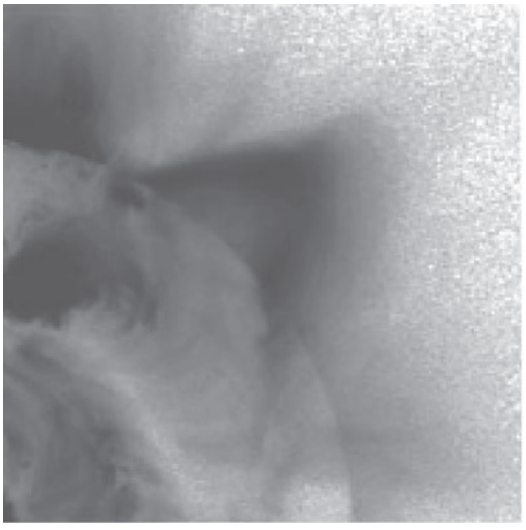

Figure 14

Soft X-ray image (negative) taken with the Soft X-ray Telescope (SXT) on the *Yohkoh* satellite during a solar flare, showing a cusp structure (Shiota et al. 2005).

the star-disk field line is wound around the polar field lines and reconnects recurrently with itself. More generally, the field lines do not need to reconnect with themselves. The shear between star and disk leads to a situation similar to **Figure 13*d*** and corresponds to twisting (**Figure 13*e***). Simulations of the evolution are discussed in Section 5.2. Reconnection restores the magnetic field to the initial configuration. In low-resistivity gas, the magnetic energy builds up continuously, but is discharged impulsively. Reconnection occurs intermittently, releasing energy that originates from rotation.

4.2. Energy Release and Acceleration

Steady reconnection by stationary inflows into a magnetic X-point has been proposed by Petschek (1964) in a 2D scenario. The region where magnetic field lines are newly connected was later found in simulations to be more extended and most likely a sheet in three dimensions (Biskamp 1986). The reality may be in between: As reconnection does not proceed uniformly over a large surface, magnetic islands develop, constricted by lines along which reconnection occurs fastest. The process occurs only at low resistivity and has been simulated numerically (Samtaney et al. 2009). Evidence for magnetic island formation has been reported in current sheets behind solar CMEs by Bemporad (2008). As plasmoids in a current sheet attract each other magnetically, secondary current sheets are formed, which may be responsible for solar radio pulsations at decimeter wavelength in solar and stellar flares (Kliem, Karlický & Benz 2000; Benz, Battaglia & Villmer 2010; see also **Figure 3**).

Acceleration of electrons and ions is ubiquitous in flares. The process enhances the particle energy from thermal emissions to several kiloelectronvolts, thus at least by a factor of 20. Two surprising properties of the accelerated particle population have been evident since the first HXR observations of nonthermal electrons. (*a*) The spectrum is nearly a power law from about 10 keV to tens of megaelectronvolts. There are deviations, however. Most common are spectra with a downward break, as is noticeable in **Figure 2**. Below about 50 keV the spectrum often becomes harder, for which there may be several reasons: reflection at the photosphere, electric field in the propagation path to the thick target, or a property of the acceleration process. At high energies, the spectrum tends to become harder (i.e., flatter), which may be due to the relativistic change

in cross-section. According to the bremsstrahlung mechanism, a power-law photon spectrum is produced by a power-law electron distribution in energy. If the electrons impinge as a beam on the chromosphere and completely lose their energy by collisions—a situation termed thick target (Brown 1971)—the power-law index of the electrons is larger than that of the bremsstrahlung photons by unity. If the electrons do not lose much energy—in a thin target—the difference is minus unity. (*b*) The power-law exponent decreases in the course of the flare, has a minimum at peak HXR flux, and increases again in late HXR emission. This is termed the soft-hard-soft behavior of HXR flare emission. It is observed in a large majority of all RHESSI flares and, surprisingly, even in subpeaks on timescales of 1 min to the resolution limit of 8 s (Grigis & Benz 2004).

Our knowledge of the nonthermal electron distributions and their energetics in stellar coronae relies mostly on the modeling of radio spectra, in particular the power-law slopes of optically thin gyrosynchrotron spectra. For a power-law electron distribution with index δ, the high-frequency gyrosynchrotron flux spectrum follows a power law $f \propto \nu^{1.22-0.9\delta}$ (Dulk & Marsh 1982). Quiescent radio gyrosynchrotron radiation from active stars shows that trapped, nonthermal electrons are continuously present; relatively hard electron distributions with $\delta \approx 2-3$ are derived from broadband spectra (e.g., Umana et al. 1993; Mutel et al. 1998; model calculations in White, Kundu & Jackson 1989). For individual flares, "spectral ageing" needs to be considered as well, because low-energy electrons are rapidly removed from the nonthermal distribution by collisions, whereas the highest-energy electrons suffer from strong synchrotron losses. Large flares on RS CVn binaries are nevertheless well fitted assuming $\delta \approx 2$ at injection time (Chiuderi Drago & Franciosini 1993). Energy considerations and the Razin limit also suggest such values for these flares (Lestrade et al. 1988).

Particle energies in stellar flares can be inferred directly from gyrosynchrotron theory if the magnetic field strength in the source is known. The latter is estimated from spatially resolved flare observations using VLBI; it is often found in the range of a few tens of Gauss for extended coronal sources (e.g., Lestrade et al. 1988; Benz, Conway & Güdel 1998; Mutel et al. 1998). Because synchrotron emission peaks at the third harmonic of $\Omega_e \gamma$, the electron gyrofrequency times the Lorentz factor, one finds that electrons with γ of order 10 (corresponding to a kinetic energy of $\approx$5 MeV) must be present in the energy distributions (Mutel et al. 1985). Further support for very high electron energies ($\gtrsim$5 MeV, or $\gamma \gtrsim 10$) comes from highly directive flare radio emission on the active K star AB Dor that can be interpreted as synchrotron radiation from ultrarelativistic particles (Lim et al. 1994). Synchrotron emission from high Lorentz-factor electrons is also suggested from millimeter flares in extended coronal regions in the T Tauri binary V773 Tau. A strong flare observed at 3-mm wavelength implies, based on a plausible surface magnetic field of 1 kG and large source sizes, Lorentz factors above 20 and up to several hundred (Massi et al. 2006).

Stellar-flare nonthermal HXR emissions have rarely been observed due to sensitivity limitations, and it is usually difficult to distinguish between a true power-law tail and the bremsstrahlung tail of a superhot thermal flare component. Osten et al. (2007) have reported >10 keV radiation from a very large flare on the RS CVn-type binary II Peg. These researchers argue in favor of a nonthermal interpretation based on the exceedingly rapid Spitzer-conductive losses for a thermal component of 300 MK (compatible with the limited signal-to-noise spectrum) and the partial presence of a Neupert effect relating SXRs and HXRs (see Section 3.4, above). The interpretation is not unequivocal, however, as for steep temperature gradients saturated heat conduction applies. Also, the presence of strong HXR emission throughout the flare, including the late decay, is at variance with solar observations. In any case, it is interesting that the nonthermal interpretation again converges to an electron power-law energy distribution with $\delta = 2.8-3.1$.

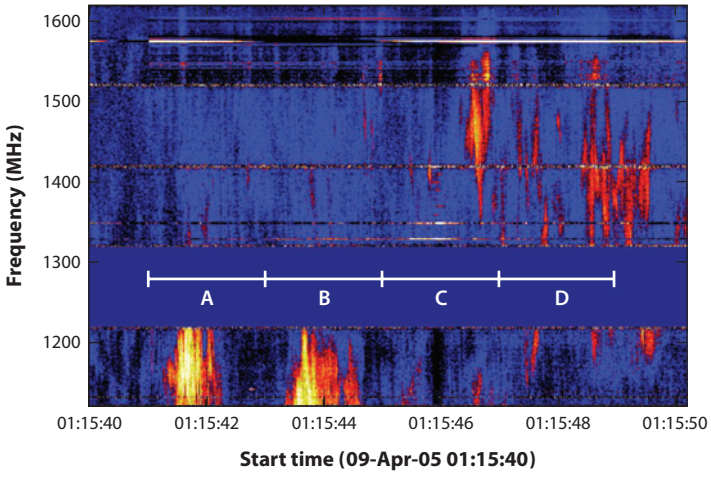

Figure 15

Dynamic spectrum of radio bursts on AD Leo (main sequence, type dM4.5e), recorded with a time resolution of 10 ms in right-circular polarization (from Osten & Bastian 2008, reproduced by permission of the AAS).

The duration of an individual acceleration process is not clear. Time structures in solar flare HXR emissions as short as 45 ms have been reported (Kiplinger et al. 1983). Radio emissions of electron beams put similar limits on the acceleration time allowing unstable beams to develop emission processes within the observed time. However, there are time structures in radio bursts that are on the millisecond timescale in bursts known as narrowband spikes and decimeter pulsations. It is not clear whether the time variations are caused by fragmented energy release or by a secondary modulation of the emission process. Similar to solar radio bursts, stellar bursts show substructures with millisecond timescales (Lang et al. 1983; Osten & Bastian 2008; see **Figure 15**). Some variant of the electron cyclotron maser (e.g., from a loss-cone or a horseshoe electron velocity distribution) has often been held responsible for these highly polarized radio bursts, perhaps occurring in an inhomogeneous medium in the case of broad-band bursts (Bastian et al. 1990, Abada-Simon et al. 1997). This hypothesis is supported by burst durations, drift rates, and collisional absorption (Osten & Bastian 2008). Given emission at the fundamental or second harmonic of Ω_e, the responsible nonthermal electron population resides in very strong coronal magnetic fields (300–600 G for 1.6 GHz radiation). From dynamic radio spectroscopy, very short (30 ms at 1.1–1.6 GHz), narrowband ($\Delta\nu/\nu \approx 5\%$), fast-drifting bursts have been identified in the active M dwarf AD Leo that bear striking similarity to solar radio spike bursts (Osten & Bastian 2006). The bursts again indicate a highly fragmented accelerator or alternatively rapid secondary modulation, one example showing up to 45 bursts per second over a time interval of about 1 min.

There are various channels through which the initial magnetic energy can be transformed into kinetic particle energy and cause acceleration. The major processes proposed for solar flare acceleration include the following:

- Stationary DC electric fields of the current sheet are natural suspects for acceleration of charged particles. Outside of the current sheet, the electric field—driven by $\mathbf{V} \times \mathbf{B}$—is perpendicular to the magnetic field and does not accelerate particles. As Faraday's law requires that the electric field inside the current sheet is the same, there is a region where the magnetic field is low and acceleration is possible. In a sheared magnetic field in three dimensions, there is an electric field component parallel to B. The accelerating particles may get lost owing to the remaining weak perpendicular field, however, before they reach high velocity. Considering the small width of current sheets, the low density in the corona, and the large number of accelerated electrons required by X-ray flare observations (up to 10^{39} s^{-1} in giant flares), it is not clear whether DC electric field acceleration can play a major role in flares

even if the particles left the tiny current sheet with the speed of light. Variants of a multitude of current sheets and dynamic current sheets with parallel electric fields have been proposed to remedy the problem.

- Shock waves are well known accelerators in astrophysics. The conversion of the energy of the piston to kinetic particle energy depends on the Mach number. Reconnection jets of flares have been proposed to create shocks both at the interface between inflowing and outflowing material and at the termination of the outflow. Acceleration by CMEs and other interplanetary shocks is well observed in situ, by remote particle detection and by radio observations. However, the acceleration efficiency reaches only 10%, and only 1% goes into electrons (Mewaldt et al. 2008). Therefore, shocks appear unlikely to be the primary acceleration process for flare electrons.
- The currently most widely discussed flare acceleration process proposes particles interacting stochastically with variable electric and magnetic wave fields. Various waves have been proposed, in particular fast (magnetoacoustic) waves in Cerenkov resonance with electrons. This acceleration mechanism is known as transit-time damping (Miller, Larosa & Moore 1996; Petrosian & Liu 2004). It is a second-order Fermi process in which particles are mirrored by wave fields and lose or gain energy depending on whether they meet a mirror head on or from the back. As head-on collisions have a higher probability, the particles gain energy on the average, following a diffusion equation in momentum space. Complemented by escape from the acceleration region and replenishment of cold particles, the equation has a stationary, near-power-law solution (Grigis & Benz 2005). The solution predicts a hardening of the nonthermal X-ray spectrum correlated with higher X-ray flux, as observed in solar flares (Grigis & Benz 2006). Waves having frequencies near the proton gyrofrequency are also candidates (Miller et al. 1997) as gyroresonance effects appear to play a role in preferential acceleration of certain ions such as ^{3}He. Even more efficient would be waves having electric field components parallel to the magnetic field. Appropriate waves are lower-hybrid waves (Benz & Smith 1987) and kinetic Alfvén waves (Arzner & Vlahos 2004). Waves at higher frequencies, such as upper-hybrid or Langmuir waves, would couple into radio waves and become observable. Only 65% of solar X-ray flares with peak flux larger than 5×10^{-5} W m^{-2} at 1 AU (classified as C5 or larger) are accompanied by emissions that may possibly be attributed to such a process (Benz et al. 2005). Thus, plasma waves near the plasma frequency can be excluded as accelerating turbulence. Waves that stochastically accelerate charged particles may result from the reconnection process directly or in the reconnection jets, where large-scale waves are predicted to decay into smaller wavelengths and higher frequency waves (Miller, Larosa & Moore 1996). However, the process may be questioned on the requirement to transfer free magnetic energy into waves at high efficiency and a fast rate. A recent prediction of stochastic acceleration that protons are accelerated in larger loops than electrons (Emslie, Miller & Brown 2004) was contradicted by observations (Hurford et al. 2006).

The absence of coherent radio emission originating from plasma wave turbulence in the acceleration region in some flares puts stringent constraints on the acceleration process. It requires that flares accelerate electrons without bringing them into an unstable momentum distribution that can drive high-frequency waves into becoming observable waves in radio emission. DC electric fields are prone to produce beams. Electron beams are particularly efficient in emitting radio waves, as are loss-cone velocity distributions resulting from magnetic trapping and shock waves (Benz 2002). Stochastic acceleration being the most gentle process of the above is best suited to comply with the requirement of occasional radio quietness. Particles diffuse out of the thermal distribution into a high-energy tail that does not emit coherent radio emission.

4.3. Energy Transport

Nonthermal X-rays originate mostly from footpoints into which nonthermal electrons precipitate. Assuming that the electrons hit a cold target and if their low-energy cutoff is known, their total energy can be calculated. The energy is some significant fraction of the total flare energy. If released in the corona, the energy has to be transported to the chromospheric target. Two means of transport are known: free-flying particles and thermal conduction. Both mechanisms transport energy along the magnetic field lines. Note that the collisional mean free path in an ionized gas increases with particle energy. In the first case, high-energy electrons or protons reach the target practically without collisions. In the second case, thermal particles, having a smaller mean free path, collide and transfer the energy to other thermal particles, which then collide again, etc.

The observed Neupert effect (Section 3.4, above) suggests that, in the impulsive flare phase, nonthermal electrons precipitate freely and transport the energy. In most flares, the high-energy electrons reach the chromosphere. Some cases have been reported where electrons <50 keV lost their energy already on the way, presumably due to a high density in the loop (Veronig & Brown 2004). The heat is then deposited in the dense loop and conducted to the chromosphere without producing X-ray footpoints.

Regular flares sometimes have a preflare phase before nonthermal footpoints appear. In the X-rays, only a source in the corona is observable (Acton et al. 1992). Fárník, Hudson & Watanabe (1996) find events with substantial thermal X-ray emission several minutes before the onset of nonthermal emission and that it is unrelated to beam-driven evaporation. RHESSI observations reveal that 90% of all flares show preflare heating lasting, on the average, 3 min before nonthermal emission sets in (Veronig et al. 2002). The increase in emission measure and density indicate that chromospheric material is flowing into the coronal source. The observed energy requirement is consistent with thermal conduction from the coronal source to the chromosphere (Battaglia, Fletcher & Benz 2009). Conduction is found to be at a saturated rate. To interpret these observations, the energy release must initially be a heating process, turning gradually into acceleration of nonthermal particles. A gentle transition from heating to acceleration is consistent with a stochastic process (Grigis & Benz 2006).

Alternatively, the initial energy may be transported into the footpoint regions by protons. A smaller number of protons is required to transport the same amount of energy, and electrons can be dragged along with the proton beam, hence the return current problem (Section 4.4, below) is alleviated (Simnett 1986, Woodgate et al. 1992). Proton beams are, however, more difficult to observe. Gamma-ray line emissions during large solar flares indicate proton beams colliding with the chromosphere, but the corresponding emission is not detectable in stars with present-day instruments. Proton beam transport would be an interesting way to explain flare emissions not correlated in the standard way (e.g., gyrosynchrotron emission preceding SXR flares, etc.). Proton beams are expected to charge-exchange with H atoms in the chromosphere, followed by Lyα emission. One therefore expects Doppler-shifted (by the beam velocity) Lyα emission toward the red wings (Orrall & Zirker 1976). This diagnostic is particularly well suited for flares in late-type stars. Woodgate et al. (1992) indeed detected excess red-wing emission during a flare in AU Mic, and estimated a proton beam energy flux of at least 10^{30} erg s^{-1} during a 3-s interval, greatly exceeding the transition region emission estimated at $\approx 10^{28}$ erg s^{-1} in the temperature range of $(4-8)\times 10^4$ K.

4.4. Return Current and Electric Field

An electric current of the density of the electron beam inferred at the HXR footpoints would induce an enormous magnetic field according to Ampère's equation. Although ions are also accelerated,

it is highly unlikely that the ion beam matches the electrons. To equilibrate the current produced by the particle beams, a return current must flow (van den Oord 1990, Benz 2002). It is nearly equal, but opposite in direction to the beam current and practically inhibits magnetic induction. It also replenishes the particles that have escaped from the acceleration region and eliminates electric charging of the acceleration region. As this return current consists of thermal electrons, it has a finite resistance produced by electron-ion collisions. Ohm's law then requires an electric field parallel to the magnetic field. If electrons dominate the beam current, the beam current goes up, and the return current flows downward. Thus, the electric field also points downward from the corona and slows down the free-flying electrons in the beam.

Energy loss by an electric field in the precipitation region is suggested by the observed nonthermal X-ray spectra differing between the coronal source and the footpoints in some solar flares. It also affects the energy distribution of the beam electrons, causing a downward kink in the photon spectrum (Zharkova & Gordovskyy 2005). The energy loss is a measure of the electric field strength and, thus, the current density. The current becomes unstable when the drift velocity of electrons exceeds the mean thermal proton velocity by about an order of magnitude. This seems to be case in the two events with observable electric field effect reported by Battaglia & Benz (2008). Instability enhances the effective collisions rate, greatly augmenting the resistivity and, thus, the electric field. Electric potentials between 10 keV and 60 keV are inferred from RHESSI observations.

4.5. Evaporation

When energy is deposited into the chromosphere by a precipitating beam or thermal conduction, the atmosphere generally expands and chromospheric material is said to evaporate into the corona. The material is tens of millions of Kelvins hot, accumulates at the top of the loops, and emits most of the thermal X-rays observed in flares. Evaporation comes in two ways: either by a slow transition into a new equilibrium or—if the heating rate is much faster than the radiation and expansion rates—by an overpressure expansion into both directions along the magnetic field. The two types of evaporation are known as gentle and explosive. Theoretical studies estimate that under solar conditions, explosive evaporation occurs if the heating flux exceeds the critical value of 3×10^{10} erg cm^{-2} s^{-1} (Fisher, Canfield & McClymont 1985; Abbett & Hawley 1999).

In the impulsive phase of solar flares, >20 MK plasma expanding with 200 to 400 km s^{-1} into the corona is observed in blueshifted CaXIX and FeXIX lines (Antonucci et al. 1982). Such expansion velocities are indicative of explosive evaporation. They are frequently accompanied by downflows at tens of kilometers per second in cooler lines. Lines such as HeI and OV v lines originating at chromospheric and transition region temperatures are observed with both positive or negative Doppler shift. Upflows between 10 and 20 km s^{-1} have also been reported (Milligan et al. 2006) in the main phase, indicating gentle evaporation by a low-particle influx. Apparently, the heating by precipitating particles is not uniform. Upflow velocities in the range of 20 km s^{-1} to 150 km s^{-1} are needed to interpret the density increase in the coronal source of the preflare phase (Battaglia, Fletcher & Benz 2009). Velocities in the preflare and late flare phases lacking HXR footpoints, when energy transport is preferentially by thermal conduction, are generally lower and in the range of gentle evaporation even in the hot lines (Brosius & Phillips 2004).

Stellar flare observations also provide strong support for the chromospheric evaporation mechanism. The Neupert effect provides the best qualitative evidence (Section 3.3, above). Quantitative information is available from high-resolution spectroscopy. The spectral resolving power available in the X-ray domain (a few hundred) is, however, marginal for the expected velocities, and the

most significant mass motion occurs in the initial phase of a flare when the X-ray emission is still quite weak.

Optical and UV spectroscopy, however, have shown blueshifted lines and blue-wing excesses during the flare onset, and redshifted lines also during the impulsive phase and additionally during the later decay phase (Houdebine et al. 1993a, Montes et al. 1999, Hawley et al. 2003, Fuhrmeister et al. 2008). An interpretation in terms of mass motion suggests velocities of a few tens of kilometers per second, sometimes up to a few hundred kilometers per second for gas heated to about 10,000 K. High velocities in blueshifted optical and UV line components, as seen in a flare on UV Cet (Eason et al. 1992) and AT Mic (Gunn et al. 1994), suggest evaporating gas. AT Mic showed upward bulk velocities of 250 km s^{-1} in blue-wing excesses of Balmer lines but also, somewhat surprisingly, in the CaII lines that form in the lower, cooler chromosphere. Apparently, the particle beam initiating evaporation must have penetrated very deeply into the chromosphere (Gunn et al. 1994) and caused rapid expansion in both directions along the magnetic field similar to solar processes, but at larger velocities. Similar line-of-sight blueshift velocities are found in the UV "coronal" FeXIII line during a flare on CN Leo (Fuhrmeister, Schmitt & Wichmann 2004), and in CIV and in Hα at the onset of flares on cool dwarfs (Montes et al. 1999, Fuhrmeister & Schmitt 2004). Although such motions are clearly not related to the bulk evaporation of hot plasma (emitting in SXRs and the EUV wavelengths), they may represent the initial upward motion and later downfall of associated prominence gas. Prominence expansion and disruption have been observed spectroscopically during the gradual phase of a flare on an M dwarf (Houdebine et al. 1993a). The blueshifted lines may also relate to CMEs (Houdebine, Foing & Rodono 1990) or part of the chromospheric evaporation, whereas the redshifts in the impulsive phase are related to "chromospheric condensation" (downward motion) during a large chromospheric energy input (Fisher 1989).

X-ray spectroscopy provides unequivocal information on coronal density changes during flare evaporation. A large flare in Proxima Centauri showed a density increase by about two orders of magnitude (with peak electron densities of a few times 10^{11} cm^{-3}) for relatively cool plasma forming at 1–4 MK. Although the primary flare plasma is hotter, this observation showed that the cool component must be continuously replenished during the flare decay, suggesting plasma that is cooling from higher temperatures to preflare levels (Güdel et al. 2002a).

Based on hydrodynamic models, an initial SXR pulse should originate during the early evaporation phase when heating due to energetic electrons is most efficient and densities rapidly increase in the lower corona, driving the hot plasma upward. A very short (decay time of $\approx$2 s) impulsive SXR burst has indeed been detected simultaneously with an optical flare peak on the late M dwarf CN Leo, both bursts preceding the main thermal X-ray flare by about 200 s (Schmitt et al. 2008).

5. FLARE EFFECTS

5.1. Coronal Heating

To keep the corona at high temperature, little energy is required compared to the energies available in the layers below. Thus, several heating mechanisms are conceivable. Here we focus on the energy provided by the impulsive release in flares. For solar active regions there are several reasons why the large flares cannot be the major cause of coronal heating: (*a*) There is a corona at times without an active region on the Sun. (*b*) The amplitude distribution of solar flares may be a power law with index below 2 (see Section 3.6, above). Thus, large flares dominate the total power in the solar corona. However, the corona does not vary in phase with large flares. (*c*) The energy in large flares is not even sufficient to support the active region radiative output, not to mention

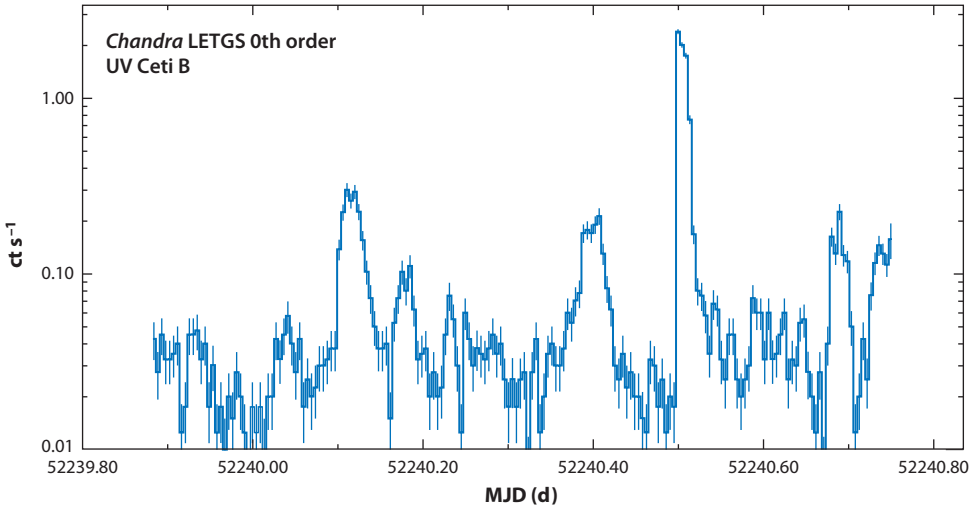

Figure 16

X-ray light curve of UV Ceti B (type dM6.0Ve), observed during about one day. Note the logarithmic flux axis (figure courtesy of M. Audard, after Audard, Güdel & Mewe 2003).

the whole corona's energy requirement. Adding up all observed microflare events, Hannah et al. (2008) and Christe & Krucker (2008) find that the average energy input by >10 keV electrons is $<10^{26}$ erg s^{-1}, less than the coronal output observed in thermal X-rays at spotless time.

The situation is different for the quiet solar corona outside of active regions. Chromospheric jets (spicules) have been observed at the limb for decades. This became more interesting when UV emission was reported from high-energy events in the transition region (Brueckner & Bartoe 1983). Finally, small X-ray flares emitted by gas at coronal temperatures were detected in quiet regions (Krucker et al. 1997), indicating nonstationary energy input. They were later also found in hot EUV lines at even lower energy and further studied in transition region EUV lines, most recently by the *Hinode*/EUV Imaging Spectrometer (EIS) (Brooks & Warren 2009, De Pontieu et al. 2009). The total input by such nanoflares is best estimated from coronal brightenings in high-temperature EUV lines. Integrated up from the low-energy instrumental threshold (SOHO/EIT), it amounts to 10%–20% of the required rate (Benz & Krucker 2002). This percentage does not include the energy input by nanoflares below resolution nor by transition region activity. Thus, the major remaining uncertainty is not the spectral index, but the total energy input into the corona by a single flare. As long as only a fraction of the energy is accounted for, the role of nanoflares in heating in the quiet solar corona will remain unclear.

In contrast, numerous observations of stellar coronae suggest flare-like processes to be responsible for coronal heating in magnetically more active stars. We first mention the ubiquitous evidence in light curves for frequent, small flares that may contribute to quasi-continuous coronal heating. "Micro-variability" is particularly well observed in X-ray or EUV light curves of active stars (e.g., Butler et al. 1986, Audard et al. 2000, Maggio et al. 2000), including very young stars (Montmerle et al. 1983, Wolk et al. 2005). In extreme cases, no nonvariable, quiescent level can be defined anymore (e.g., Audard, Güdel & Mewe 2003; **Figure 16**). Correlated time behavior in low-level flaring has been observed for EUV and Hγ emission (Butler, Rodono & Foing 1988), and for X-rays and U-band emission (Güdel et al. 2002a); in the latter case, the Neupert effect was often evident, clearly identifying these events as flares. Marino, Micela & Peres (2000) analyzed the light curve luminosity distribution of active stars over timescales from hours to days and found the distribution to resemble the equivalent distribution of solar flares, indicating that the stellar light curves are composed of contributions from many solar-like flares. Micro-variability is also

seen at radio wavelengths; rapidly varying, highly polarized emission at 1.4 GHz from RS CVn-type binaries has been interpreted as the plasma radiation induced by high-cadence acceleration events (White & Franciosini 1995). Continuous variability of the gyrosynchrotron component is seen during ≈30% of the time, on timescales of tens of minutes. The number of events increases toward lower flux amplitude (Lefèvre, Klein & Lestrade 1994), as also evidenced in long radio light curves obtained for Algol and HR 1099 by Mutel et al. (1998).

If the detected total flare energy is not sufficient for heating, events below the resolution may be proposed. The small events are particularly attractive if the power-law index $\alpha > 2$ for the flare energy distributions. This is the case for most magnetically active stars studied so far (Section 3.6, above). Synthetic methods in which light curves are constructed based on flare distributions indicate that as much as 50%–80% of the apparently constant X-ray emission can well be explained by the extrapolation of the energy distribution to smaller flares (Kashyap et al. 2002). The smallest flares thus to be invoked have radiated X-ray/EUV energies typically in the range of 10^{29}–10^{30} erg for nearby active stars or about two orders of magnitude smaller than the smallest flares explicitly detected in the light curves (Kashyap et al. 2002, Güdel et al. 2003), which is still in the range of regular solar flares.

In the case of small flares heating the corona, we expect hot plasma to be continuously present. This has recently been reported for solar active regions continuously showing plasma of 6–10 MK (McTiernan 2009, Schmelz et al. 2009). Stellar X-ray observations of active stars also reveal substantial amounts of plasma persisting at temperatures exceeding 10 MK. The distribution of emission measure for a given coronal source increases in temperature (typically showing a power-law dependence) up to a characteristic peak at a temperature that is a function of "magnetic activity level" (Güdel, Guinan & Skinner 1997). The decrease beyond the peak also has the form of a power law. Such distributions can be modeled by integrating emission measures of flares in time from flare onset, when the hottest plasma is produced, to the late decay when the plasma has cooled (Güdel, Guinan & Skinner 1997; Reale et al. 2001). The observed emission measure distributions require a power-law flare energy distribution (Section 3.6, above) with $\alpha > 2$ in close agreement with values derived from other diagnostics (Güdel et al. 2003). The SXR emission measure distributions of young solar analog stars indeed suggest very similar values for α as inferred from direct light curve analysis (Telleschi et al. 2005).

Another enigma related to active stars is the persistent nonthermal radio (mostly gyrosynchrotron) radiation observed from late-type active stars. It is proportional to SXR emission, showing the same ratio as in flares (Güdel & Benz 1993 and **Figure 11**; see Section 3.5, above). Gyrosynchrotron emission is found only in stars that also show hot (≈10 MK) plasma in X-rays (Telleschi et al. 2005). Typical loss times due to radiation, collisions, or scattering require a frequent cadence of acceleration events, on timescales of minutes to hours, to replenish the high-energy electron population (Kundu et al. 1987; Lefèvre, Klein & Lestrade 1994).

We have also mentioned a number of further correlations between stellar emissions, indicating a relationship of flares and the apparently quiescent stellar atmosphere (e.g., SXR versus Mg II, Hγ, or U-band band flux) and correlations that link the radiative output of flares with quiescence (e.g., power in optical or X-ray flares versus quiescent X-rays, Section 3.5 above), which provide further support for an intimate connection between the "nonflaring" stellar atmospheres and the ensemble of flares. A general conditioning of a stellar atmosphere for flare productivity was pointed out by Cassak, Drake & Shay (2006), who find observational evidence that solar and stellar coronae are in the critical state where magnetic reconnection is close to the transition to the collisionless mode (Section 4.1, above).

Finally, we mention that average coronal densities tend to be higher in magnetically active main-sequence stars than in their inactive counterparts (Ness et al. 2004; Testa, Drake & Peres

2004). As flares produce high-density plasma at least around peak time, a high occurrence rate of small flares could mock a constantly high density in quiescent coronae. Because the emission measure scales with n_e^2, the dense hot plasma may dominate the X-ray radiation, which is often the case in active stars.

Why are there "larger flares" on magnetically more active stars that may heat their coronae? A possibility is that the higher packing of magnetic active regions, also implying smaller magnetic field divergence with increasing height and, therefore, stronger (nonpotential) magnetic fields, may be susceptible to more frequent and more energetic reconnection events (Güdel, Guinan & Skinner 1997).

5.2. Coronal Mass Ejections and Shock Waves

Cusp-shaped reconnection configurations (**Figure 13*a***) suggest a reconnection jet in upward direction. This jet is closely related to the flare and driven by magnetic forces. Conversely, the rise of a plasmoid may occur independently and be accompanied by reconnection later. Both scenarios seem to occur, suggesting that flares and CMEs are related. Not every flare ejects coronal material to interplanetary space. There are many more flares than plasmoids observed in interplanetary space. However, CMEs may occur without observable flares and the eventual reconnection behind the ejected blob may be a minor process.

CMEs in the solar corona are well known to accelerate until they reach an altitude of a few photospheric radii. The observed acceleration indicates that CMEs are not explosions, but are driven by the magnetic field and internal pressure. CMEs with high speed are usually accompanied by coherent radio emission of type II at a wavelength of meters and more. The radio emission is generally interpreted as a signature of electron acceleration at a super-Alfvénic shock. The comparison of white-light observations by the new *Solar Terrestrial Relations Observatory* with radio data indicates that the CMEs form a shock at an altitude of 0.5 solar photospheric radii from the Sun center (Gopalswamy et al. 2009).

Emslie et al. (2004) find an order of magnitude lower total energy released in the flare than observed in the kinetic energy of the CME. The flare energy was later revised, however, in view of the recently discovered white-light flare emission at a value comparable to the CME (Emslie et al. 2005).

Coronal mass ejections may be observed as excessive X-ray absorption during large stellar flares (Ottmann & Schmitt 1996, Tsuboi et al. 1998, Favata & Schmitt 1999). This absorption may indicate the presence of cool mass flowing behind the CME as observed sometimes in the solar atmosphere in the form of a rising prominence. Evidence for ejections can also be seen in blueshifted Hα emission features in SXR flares (Fuhrmeister & Schmitt 2004, Montes et al. 1999; **Figure 17**). Houdebine et al. (1993b) provide a quantitative assessment of the energetics of mass motions during a flare on the M dwarf AD Leo based on optical/UV lines. They interpret pre-ejection blueshifts as being related to "dark filaments," and impulsive-phase redshifts resulting from "chromospheric condensation" motions in the chromosphere. Gradual-phase quasi-periodic Doppler shifts may be caused by oscillations in an erupting prominence, and large blueshifts (140 km s^{-1}) in the late gradual phase by prominence eruptions. The total kinetic energy in these flare-related mass motions is estimated to exceed the total radiated energy in the U band by a factor of three. Evidence for a subsequent CME with a kinetic energy another factor of 100 higher ($\approx 5 \times 10^{34}$ erg for maximum line-of-sight velocities of 5,800 km s^{-1}) was reported for the same flare (Houdebine, Foing & Rodono 1990).

CMEs may, in their initial phase, also leave a signature in slowly decaying EUV emission after giant stellar flares, as demonstrated by Cully et al. (1994) for the dMe star AU Mic using a

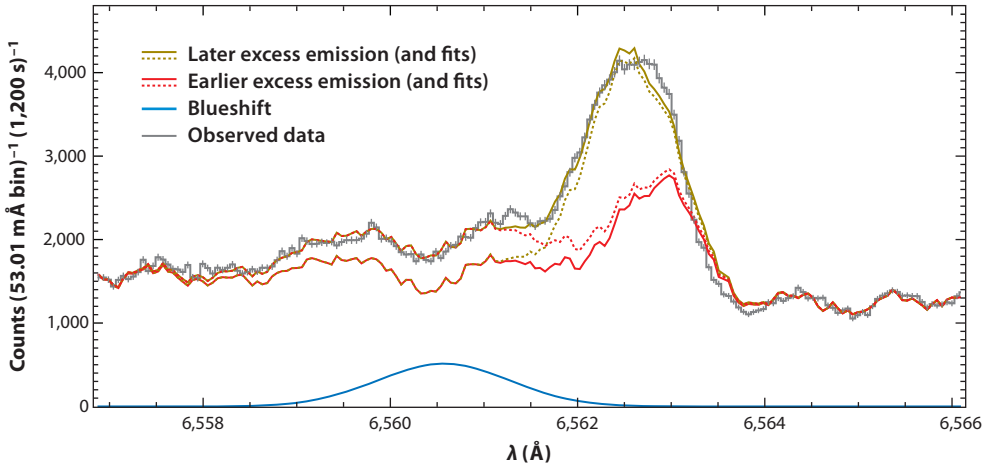

Figure 17

Strongly blueshifted component in the Hα line during the late phase of a flare on an M9 dwarf star. The middle solid line (*red*) shows a spectrum taken at an earlier time during the flare, whereas the upper solid line (*yellow*) shows a fit to the excess emission during the later phase (observed data are shown by the gray histogram with error bars). The dotted line (*yellow*) show the fits to the unshifted excess emission above the lower spectrum. For clarity, the strongly blueshifted excess Gaussian is plotted separately in the lower part of the figure (*blue*). Its blueshift corresponds to a line-of-sight velocity of $\approx$100 km s^{-1} and is interpreted in terms of emission from a mass ejection (courtesy of B. Fuhrmeister, after Fuhrmeister & Schmitt 2004).

simple model of a magnetically confined, expanding plasmoid. These researchers find approximate equality of the thermal energy and the kinetic plasmoid energy ($\approx 10^{36}$ erg each, for a 10^{20}-g ejection).

As discussed earlier (Section 4.1, above), reconnection occurs in star-disk connecting fields (**Figure 13*f***) if the rotation rates of stellar surface and disk differ (review by Uzdensky 2004). Hayashi, Shibata & Matsumoto (1996) simulated the development of initially poloidal star-disk fields subject to rotational twist (**Figure 18**). Magnetic fields rise and develop cusps that are blown open after reconnection, ejecting plasmoids that may contribute to jet outflows. This model was further developed to interpret giant, quasi-periodic X-ray flares in a disk-surrounded protostar (Montmerle et al. 2000; Yelenina, Ustyugova & Koldoba 2006). In 2D projection (**Figure 18**), the magnetic configuration corresponds to a cusp-like reconnection.

5.3. Flares and Circumstellar Disks

The final step of material accretion onto T Tauri stars and protostars is thought to proceed along magnetic field lines that connect the star with the inner border of the circumstellar disk near the corotation radius (Shu et al. 1994). Interactions between magnetic fields, accretion streams, and circumstellar disks are particularly relevant in the context of flares occurring in these regions.

Protostars and T Tauri stars of class I and older have extremely strong X-ray flares (Tsuboi et al. 1998, Wolk et al. 2005) with X-ray luminosities up to 10^{34}–10^{36} erg s^{-1} (Grosso et al. 1997; see Güdel 2004 for a list of references having further examples). Such flares cannot, on energetic grounds, occur in very compact active regions as on the Sun or they would imply exceedingly high densities that would drain the available energy very rapidly by radiation, contrary to the

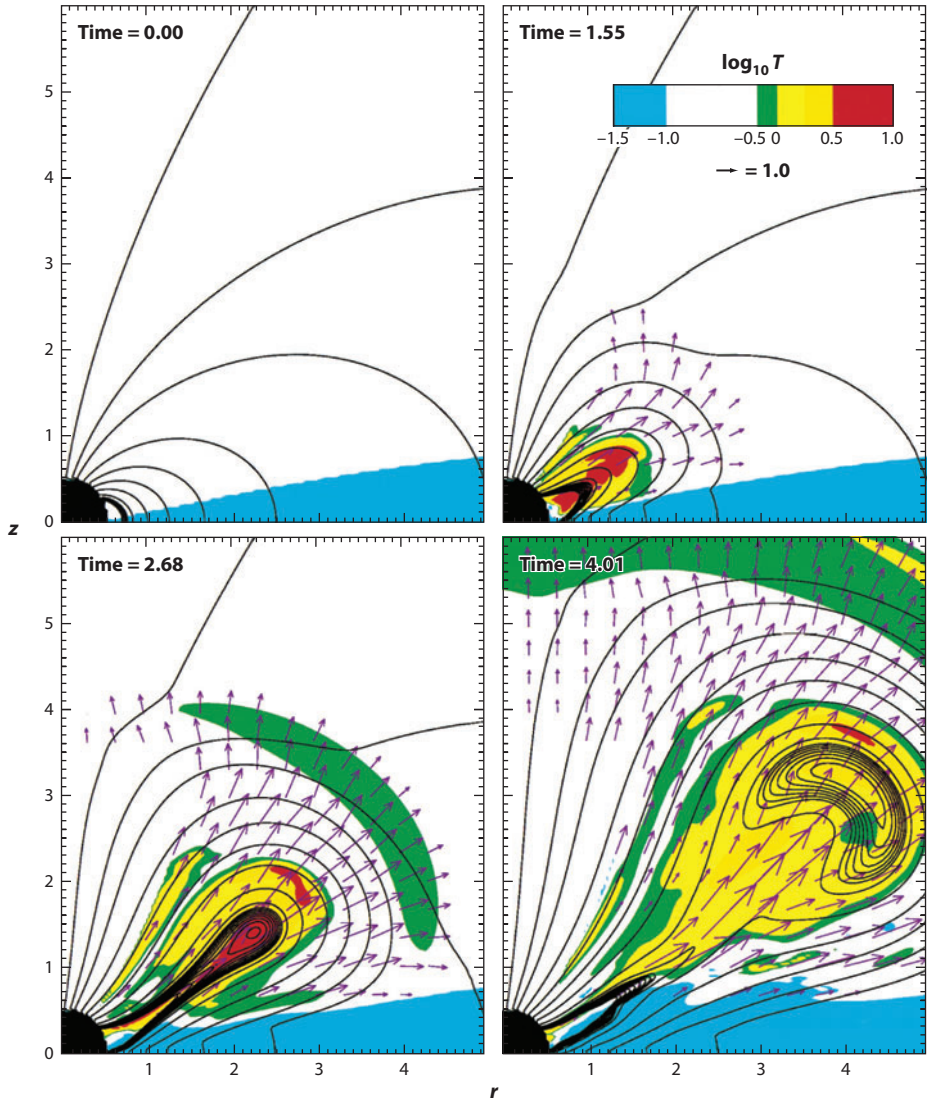

Figure 18

Plasmoid ejection after magnetic field disruption as a consequence of twisted magnetic fields (*black curves*) between star and disk. The color shows temperature (in units of 1/3 initial coronal temperature) as coded in the bar at upper right. The spatial dimensions are given in units of the radius at disk pressure maximum. Arrows indicate direction and magnitude of flow velocity. The velocity unit is defined by the orbital velocity at disk maximum pressure and indicated by an arrow at the top right. Time is given in units of orbital period at the radius of disk pressure maximum (from a simulation by Hayashi, Shibata & Matsumoto 1996, reproduced by permission of the AAS).

observed long timescales. The involved magnetic structures may reach out to the inner border of the circumstellar disk as inferred from simple estimates and scaling laws (Grosso et al. 1997, Favata et al. 2005) and radio observations as discussed in Section 4.1. In other words, star-disk magnetic fields may be a place of energy release by magnetic reconnection as discussed in Sections 4.1 and 5.2 (**Figure 18**). Loop heights inferred from simple scaling laws indeed appear to be bounded by the corotation radius in disk-surrounded stars (i.e., the inner disk radius), different from diskless systems (Getman et al. 2008). In a contrasting view, however, Imanishi et al. (2003) inferred flaring sizes of order of the stellar radius based on MHD considerations, both for T Tauri stars and protostars.

Hydrodynamic simulations of flares occurring in star-disk magnetic loops suggest that evaporation is driven from both the stellar chromosphere/transition region and the disk surface

(Isobe et al. 2003). If the flare energy input is sufficiently high, implying that the temperature gradients become sufficiently large, the entire disk may evaporate at the magnetic loop footpoint, and the opposite magnetic loop leg may then be heated as well. In the simulations, full disk evaporation is reached for flare peak temperatures of order 10^8 K. It is nevertheless remarkable that the observable signatures of such star-disk flares are difficult to distinguish from pure stellar flare signatures.

This unfortunate situation is reflected in observations. Statistical distributions of principal flare properties (duration, temperatures, X-ray luminosities, etc.) appear to be similar for accreting and nonaccreting/diskless T Tauri stars (Getman et al. 2008); the physical flare processes are similar in both types of stars although somewhat more energetic flares appear to be present in disk-surrounded stars (Imanishi et al. 2003), and extremely hard spectra are observed from large flares in such objects (Getman et al. 2008).

5.4. Flares, Protons, and Circumstellar Solids

Flare-like events in the young, pre-main-sequence Sun may have had far-reaching consequences for the processing of circumstellar, protoplanetary material. Of specific interest in this context are chondrules and isotopic anomalies in chondritic meteorites. The former are millimeter-sized spheres of igneous rock that required heating to melting temperatures for an hour or less. "Calcium-aluminum-rich inclusions (CAIs)" are meteoritic structures that may also derive from melts or partial melts. They contain evidence for short-lived radionuclides in the young Solar System, such as ^{26}Al or ^{41}Ca. These isotopes could have been injected by external nucleosynthetic events (ejecta from asymptotic giant branch stars, Wolf-Rayet stars, supernova explosions) during the formation of the Solar System, but such injection sources are rarely close to forming stars, and incorporation of the radionuclides into CAIs requires a very short time interval ($\approx 10^5$ years or less), in turn requiring a very fast trigger for solar-system formation (Lee et al. 1998).

Alternatively, high-energy protons ("solar cosmic rays") accelerated in local flares may produce the relevant radionuclides. A highly active young Sun is indeed suggested from enrichments of spallation-produced ^{21}Ne and ^{38}Ar in meteoritic grains that show radiation damage trails from solar flare nuclei (Caffee et al. 1987). In the *x*-wind theory of Shu et al. (1997), magnetic reconnection flares are produced at the inner border of the circumstellar disk close to the corotation radius (where the disk orbit period equals the stellar rotation period). Reconnection events can occur in magnetic fields that shear across the disk midplane in this region. Flare protons could then synthesize radionuclides locally, radiative heating could flash-melt material, e.g., by X-ray heating, and the *x*-wind could transport the irradiated material to larger distances. Alternatively, the strong flaring activity of protostars and T Tauri stars themselves could provide the required proton flux. From observations of the Orion Nebula region and scaling with the present-day Sun, Feigelson, Gamire & Pravdo (2002) estimated a proton flux around low-mass YSOs about 10^5 times higher than at present. Such elevated proton fluxes are indeed required to explain the observed radionuclide abundances in meteorites (Lee et al. 1998). There is some discrepancy between ^{41}Ca and ^{26}Al production, requiring, for the latter, bombardment by ^{3}He, which is typically produced in solar impulsive flares. Also, the case of ^{60}Fe remains unexplained and may require stellar nucleosynthesis or a supernova explosion (see Lee et al. 1998 and references therein). Although promising, local production of radionuclides in flares around the young Sun may not be responsible for all isotopic anomalies in meteorites (Goswami, Marhas & Sahijpal 2001).

5.5. X-Ray and Far Ultraviolet–Driven Circumstellar Chemistry and Ionization

Far UV (FUV): photons in the range of 6 eV to 13.6 eV, thus 91.2 nm to 207 nm; they ionize some atoms and molecules, but not hydrogen

Ionization changes the gas phase chemistry in environments of protostars dramatically due to the long-range potential of ionized molecules. Reactions between positively ionized and neutral molecules play a major role in the molecular evolution of star-forming regions (Herbst & Klemperer 1973, Dalgarno & Black 1976). There is often no activation barrier, and reactions are usually exothermic. New and rapid reactions become possible even at densities below 10^4 cm^{-3}. Even reactions with H_2, which is usually not reactive at low temperature, occur at a fast rate. H_2 being the most abundant molecule, the most important reactions are

$$H_2 + \gamma \rightarrow H_2^+ + e^-$$

and

$$H_2^+ + H_2 \rightarrow H_3^+ + H.$$

H_3^+ is the starting point for the evolution of the oxygen, carbon, and nitrogen chemistries.

There is a low-level, ubiquitous ionization rate in star-forming regions produced by galactic cosmic rays of some 5×10^{-17} s^{-1}. High-energy cosmic rays, both galactic and protostellar, penetrate the densest part of circumstellar disks and keep ionization and heating at a low level. Ionization and recombination reach an equilibrium.

Flare-produced X-rays enhance the ionization significantly near YSOs. The cross section for photons with energies above 10 keV is less than 10^{-24} cm^2. Thus, they may escape from protostellar envelopes if they do not penetrate a disk. Finally, geometric dilution diminishes the photon flux such that the ionization rate equals the cosmic ray level at 5,300 AU for an X-ray luminosity of 10^{32} erg s^{-1} (Stäuber et al. 2005). X-ray photons with energies below 10 keV are usually absorbed in the envelope rather than diluted. At surfaces of the molecular gas to a compact HII region or an outflow, FUV radiation dominates the ionization rate. Thus, it plays an important role at outflow walls and disk surfaces. FUV originates from accretion hot spots and from the stellar photosphere in high-mass protostars. It penetrates typically a column density of 10^{21} cm^{-2}, i.e., more than two orders of magnitude less than for X-rays. The various irradiation zones are depicted in **Figure 19**. Where the temperature exceeds the H_2O evaporation point around 100 K, water ice and any complex molecule trapped in it during the cold collapse change into gas phase. The result is a hot core with a plethora of large-molecular species (Herbst & van Dishoeck 2009).

The relatively HXR radiation from flares also alters structure, chemistry, and the ionization of circumstellar disks. The larger penetration depth of harder X-rays during flares may lead to the complete disappearance of dead zones containing cool, neutral gas near the mid-plane of the disk, at least at distances of order 1 AU from the central star (Ilgner & Nelson 2006). For larger stellar distances, the effect of flares is to add a (time-averaged) level of radiation. Flaring radiation may therefore significantly alter the accretion behavior through ionization, which drives the magnetorotational instability (Ilgner & Nelson 2006). Bursts of high X-ray flux also heat the molecular gas, raising its temperature and driving further molecular evolution.

5.6. Flares and Planetary Atmospheres

Stellar magnetic activity has a profound influence on young planetary atmospheres. For example, although the young zero-age main-sequence Sun was bolometrically 30% fainter than at present, its magnetic activity was enhanced as a consequence of its higher rotation rate. Studies of solar analogs at different ages indicate a radiation level ≈1,000× , ≈100× , and perhaps 10× the present level in the SXR range, the EUV range, and the UV range (Güdel, Guinan & Skinner 1997; Ribas

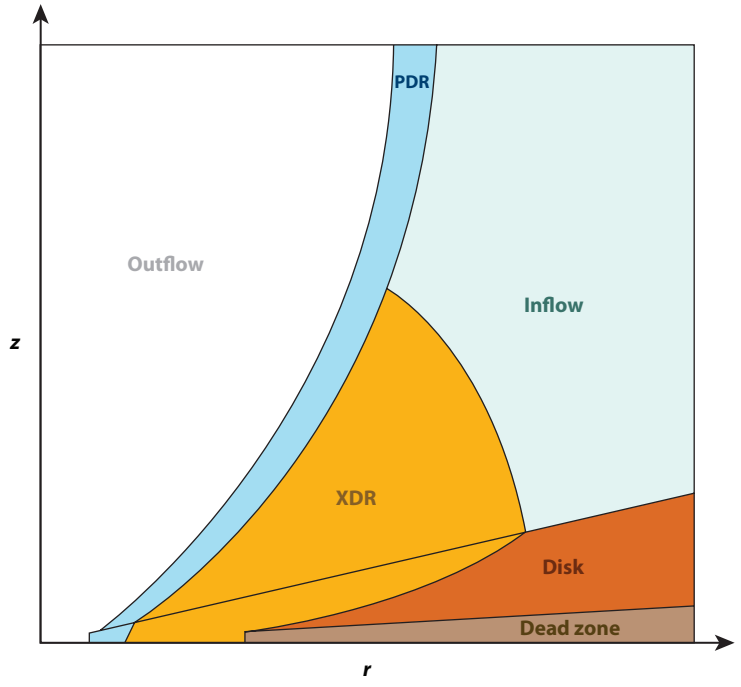

Figure 19

Schematic cut through a star-disk-envelope geometry showing various irradiation zones of a young stellar object. PDR denotes the photodissociation region, where far-UV irradiation dominates chemistry. XDR is the X-ray dissociation region, where X-rays have a larger effect than cosmic ray irradiation. In the dead zone, stellar irradiation is shielded by the disk.

et al. 2005). The correspondingly higher irradiation level at the top of young planetary atmospheres leads to higher heating rates in the thermospheres and to important photochemical reactions. For example, water in the upper atmosphere can be dissociated to produce H and O. Light elements, in particular H, will leave the gravitational potential (i.e., evaporate) if their kinetic energy is higher than the gravitational binding energy and the mean free path in the outer atmosphere (the exosphere) is larger than the scale height. Intense irradiation of young planetary atmospheres may thus lead to the escape of large amounts of water, a process that is held responsible for the lack of substantial amounts of water on Venus. For a review of these mechanisms, see Chassefière & Leblanc (2004), Kulikov et al. (2007), and Lundin, Lammer & Rebus (2007). Additionally, the solar wind, also thought to be enhanced in young, magnetically active stars, interacts with the upper planetary atmospheres, in particular ions, through various processes that may erode the atmosphere further. Strong planetary magnetospheres can protect the upper atmospheres from eroding interactions with the solar wind. This may have helped retain large amounts of water on Earth.

Planets closer to the parent star, and specifically planets in the "habitable zone" around low-mass M dwarfs, rapidly evolve toward slow, tidally locked rotation (i.e., the rotation period becomes equal to the orbital period). As a consequence, the dynamo-generated planetary magnetic moment will be much smaller; therefore, the ram pressure of the solar/stellar wind compresses the magnetosphere sufficiently to expose the upper atmosphere to the wind, in turn reducing magnetic protection (Grießmeier et al. 2005, Lammer et al. 2007). The smaller and weaker magnetosphere will lead to a higher cosmic ray flux at the top of the atmosphere (Grießmeier et al. 2005).

Flares may enhance the average irradiance of planetary atmospheres considerably. Although ordinary flares on the Sun do not modify planetary atmospheres in a significant way (apart from "ionospheric disturbances," additional ionization at ionospheric levels, and aurorae), giant flares may be more of a concern to habitable and inhabited planets. As Schaefer, King & Deliyannis (2000) showed, "superflares" with total radiated energies of order 10^{35}–10^{38} erg (in X-rays or

optical bands), i.e., 1–4 orders of magnitude more than the most energetic solar flares today, occur not only on active binaries or extremely young stars (Section 2.2), but they have been observed on solar-analog single stars, even old ones. Although their recurrence time must be long (decades to centuries), some of these flares may exceed the total irradiation input by the whole star for maybe an hour. Temporary excess heating, break-up of the ionosphere, and build-up of nitrous oxides at high altitudes may be the result. The latter destroy ozone for a long time after the flare event; Schaefer, King & Deliyannis (2000) estimate that an event with 10^{36} erg of ionizing energy results in 80% of ozone loss for more than a year, thus increasing the UV irradiation of the planetary surface from normal stellar emission. This obviously will have some impact on existing life.

CMEs add a major force of atmospheric erosion. A sufficiently high CME flux (several per day) can essentially act like an enhanced solar wind and therefore further compress planetary magnetospheres and erode the upper atmospheres (Khodachenko et al. 2007). The combination of enhanced exospheric heating by EUV irradiation with consequent exospheric expansion and a CME "wind" will lead to substantial atmospheric erosion. Pressure losses amount up to tens of bars for close-in planets (Lammer et al. 2007). This may be particularly important for planets in the habitable zones around M dwarfs.

The fluctuating UV, EUV, and X-ray irradiation as well as elevated particle fluxes (stellar "cosmic rays") from a frequently flaring star may have profound effects on planetary photochemistry, the stability of atmospheres, and eventually the formation and evolution of life on habitable planets, though details remain to be studied (see Scalo et al. 2007 for an overview). Although flare-produced gamma rays, X-rays, and EUV radiation will usually not propagate to the surface of planets bearing any substantial atmospheres, a fraction of the hard radiation will be reprocessed and re-emitted as UV light that showers the planetary surface, possibly at biologically relevant doses (Smith, Scalo & Wheeler 2004). Such elevated, variable UV radiation may have damaging effects on living cells, but may also act as an evolutionary driver.

SUMMARY POINTS

1. There is a large number of configurations that may lead to magnetic field lines prone to reconnect. In a 2D view, the field lines must be oppositely directed, but in three dimensions, magnetic shear can be sufficient. The actual process of magnetic energy release does not depend on the large-scale configuration and its driver.
2. Flares caused by magnetic reconnection release a significant fraction if not the majority of the energy into accelerated particles. The acceleration process is still disputed. Many, but not all, of the new observations in the past ten years concur with a stochastic process that lets electrons and ions diffuse to higher energy.
3. In the low-density coronae of the Sun and stars these particles are collisionless. They are not thermalized until they precipitate to the chromosphere and the corona where they heat the plasma. The coupling between chromosphere and corona is important to understand the dynamics of the gradual phase of flares.
4. The major sites of HXR emission are coronal loop footpoints in the chromosphere. However, imaging solar HXR events has demonstrated that sources in the corona during flares are common. They are possible sites of energy release and particle acceleration. The magnetic connection between coronal sources and footpoints appears to be well established.

5. Coronal heating by flares is well documented for active stars, where the quiescent X-ray emission is resolved into continuous flaring. However, the so-far observed regular flares and microflares in solar active regions do not supply the energy needed for their coronal heating. As heating is observed to strongly depend on the magnetic field strength, a decisive contribution by unresolved microflaring cannot be excluded. In the quiet Sun, the situation is also not settled. A significant fraction of the energy required to heat the corona is observed in the nanoflares in the solar corona. Waves and bulk motions injected from explosive events in the transition region may also contribute significantly.
6. Gigantic flares releasing 10^4 times the energy of present-day solar events and at many orders of magnitude higher frequency may have a significant impact on the chemistry and ionization of protoplanetary disks. Such flares and associated mass ejections are also relevant for the heating and erosion of upper planetary atmospheres and can contribute to the loss of large amounts of water.

FUTURE ISSUES

1. A major uncertainty in the flare energy input into the solar corona and to the solar SXR emission is the primary partition of the energy into particle acceleration and bulk motion. Much of the latter will be thermalized or transformed to wave energy. It is not known how and when this occurs. The importance of waves is demonstrated by the near absence of cool regions in the corona (except for thermal instabilities such as in prominences). Waves can transport the energy from the release site across the magnetic field and to higher altitudes where flares are rare. Estimates of flare energy input into the corona are uncertain by an order of magnitude if the wave output of nanoflares and explosive events is unknown.
2. HXR emission is a primary source of information for solar flares, but remains essentially undetected in stellar flares. It is a high priority for the latter to have more sensitive observations in the spectral region of 10–100 keV in the future.
3. Radio emission and nonthermal X-rays both originate from accelerated electrons. Yet, their correlation is not well known even for solar flares. New instrumental capabilities for radio observations of YSOs are coming up. Of special interest are dynamic spectra of coherent emissions as well as broadband incoherent (gyrosynchrotron) emission showing the turnover frequency. Such observations will be useful to estimate the magnetic field strength.
4. The effects of flare particles precipitating onto protoplanetary disks have not yet been sufficiently investigated.
5. Higher spectral resolution in SXR lines will provide information on motions of hot flare plasma in solar and stellar flare release sites.

DISCLOSURE STATEMENT

The authors are not aware of any affiliations, memberships, funding, or financial holdings that might be perceived as affecting the objectivity of this review.

ACKNOWLEDGMENTS

The authors thank R.P. Lin, S. Krucker, S. Mohanty, and E.F. van Dishoeck for critically reading an early version of the manuscript and comments. Flare research at ETH Zurich is supported by Swiss NSF grant 200020–121676.

LITERATURE CITED

Abada-Simon M, Lecacheux A, Aubier M, Bookbinder JA. 1997. *Astron. Astrophys.* 321:841–49
Abbett WP, Hawley SL. 1999. *Ap. J.* 521:906–19
Acton L, Tsuneta S, Ogawara Y, Bentley R, Bruner M, et al. 1992. *Science* 258:618–25
André P, Montmerle T, Feigelson ED, Stine PC, Klein KL. 1988. *Ap. J.* 335:940–52
Antonucci E, Gabriel AH, Acton LW, Leibacher JW, Culhane JL, et al. 1982. *Solar Phys.* 78:107–23
Arzner K, Vlahos L. 2004. *Ap. J. Lett.* 605:L69–72
Aschwanden MJ. 2002. *Particle Acceleration and Kinematics in Solar Flares*. Dordrecht, Netherlands: Kluwer Acad. Publ. 227 pp.
Aschwanden MJ, Kosugi T, Hanaoka Y, Nishio M, Melrose DB. 1999. *Ap. J.* 526:1026–45
Aschwanden MJ, Tarbell TD, Nightingale RW, Schrijver CJ, Title A, et al. 2000. *Ap. J.* 535:1047–65
Audard M, Güdel M, Drake JJ, Kashyap VL. 2000. *Ap. J.* 541:396–409
Audard M, Güdel M, Mewe R. 2001. *Astron. Astrophys.* 365:L318–23
Audard M, Güdel M, Skinner SL. 2003. *Ap. J.* 589:983–87
Ayres TR, Brown A, Osten RA, Brown A. 2001a. *Ap. J. Lett.* 562:L83–86
Ayres TR, Osten RA, Brown A, Huenemoerder DP, Drake JJ, et al. 2001b. *Ap. J.* 549:554–77
Bale SD, Mozer FS, Phan T. 2002. *Geophys. Res. Lett.* 29:33–36
Bastian TS, Benz AO, Gary DE. 1998. *Annu. Rev. Astron. Astrophys.* 36:131–88
Bastian TS, Bookbinder J, Dulk GA, Davis M. 1990. *Ap. J.* 353:265–73
Battaglia M, Benz AO. 2006. *Astron. Astrophys.* 456:751–60
Battaglia M, Benz AO. 2008. *Astron. Astrophys.* 487:337–44
Battaglia M, Fletcher L, Benz AO. 2009. *Astron. Astrophys.* 498:891–900
Battaglia M, Grigis PC, Benz AO. 2005. *Astron. Astrophys.* 439:737–47
Bemporad A. 2008. *Ap. J.* 689:572–84
Benz AO. 2002. *Plasma Astrophysics: Kinetic Processes in Solar and Stellar Coronae*, Vol. 279. Dordrecht, Netherlands: Kluwer Acad. Publ. 324 pp. 2nd ed.
Benz AO. 2008. *Living Rev. Solar Phys.* 5:1–64
Benz AO, Battaglia M, Villmer N. 2010. *Astron. Astrophys.* In press
Benz AO, Conway J, Güdel M. 1998. *Astron. Astrophys.* 331:596–600
Benz AO, Grigis PC, Csillaghy A, Saint-Hilaire P. 2005. *Solar Phys.* 226:121–42
Benz AO, Güdel M. 1994. *Astron. Astrophys.* 285:621–30
Benz AO, Krucker S. 2002. *Ap. J.* 568:413–21
Benz AO, Smith DF. 1987. *Solar Phys.* 107:299–309
Berger E. 2006. *Ap. J.* 648:629–36
Biskamp D. 1986. *Phys. Fluids* 29:1520–31
Bower GC, Plambeck RL, Bolatto A, McCrady N, Graham JR, et al. 2003. *Ap. J.* 598:1140–50
Bowyer S, Drake JJ, Vennes S. 2000. *Annu. Rev. Astron. Astrophys.* 38:231–88
Brinkman AC, Behar E, Güdel M, Audard M, den Boggende AJF, et al. 2001. *Astron. Astrophys.* 365:L324–28
Brooks DH, Warren HP. 2009. *Ap. J. Lett.* 703:L10–13
Brosius JW, Phillips KJH. 2004. *Ap. J.* 613:580–91
Brown JC. 1971. *Solar Phys.* 18:489–502
Brueckner GE, Bartoe J. 1983. *Ap. J.* 272:329–48
Butler CJ, Rodono M, Foing BH. 1988. *Astron. Astrophys.* 206:L1–4
Butler CJ, Rodono M, Foing BH, Haisch BM. 1986. *Nature* 321:679–82
Caffee MW, Hohenberg CM, Swindle TD, Goswami JN. 1987. *Ap. J. Lett.* 313:L31–35
Cassak PA, Drake JF, Shay MA. 2006. *Ap. J.* 644:L145–48

Cassak PA, Drake JF, Shay MA. 2008. *Ap. J.* 676:L69–72
Chassefière E, Leblanc F. 2004. *Planet. Space Sci.* 52:1039–58
Cheng C, Pallavicini R. 1991. *Ap. J.* 381:234–49
Chiuderi Drago F, Franciosini E. 1993. *Ap. J.* 410:301–8
Choi CS, Dotani T. 1998. *Ap. J.* 492:761–66
Christe SD, Krucker S. 2008. *AGU Fall Meet. Abstr.* SH13A-1510
Crosby NB, Aschwanden MJ, Dennis BR. 1993. *Solar Phys.* 143:275–99
Culhane JL, Hara H, Watanabe T, Matsuzaki K, Harra LK, et al. 2008. In *First Results From Hinode*, ed. SA Matthews, JM Davis, LK Harra, 397:121–25. San Francisco: Astron. Soc. Pac. Conf. Ser.
Cully SL, Fisher GH, Abbott MJ, Siegmund OHW. 1994. *Ap. J.* 435:449–63
Dalgarno A, Black JH. 1976. *Rep. Prog. Phys.* 39:573–612
Dennis BR, Zarro DM. 1993. *Solar Phys.* 146:177–90
De Pontieu B, McIntosh SW, Hansteen VH, Schrijver CJ. 2009. *Ap. J. Lett.* 701:L1–6
Ding MD, Fang C. 2000. *MNRAS* 317:867–72
Donati JF, Morin J, Petit P, Delfosse X, Forveille T, et al. 2008. *MNRAS* 390:545–60
Doyle JG, Butler CJ. 1985. *Nature* 313:378–80
Dulk GA, Marsh KA. 1982. *Ap. J.* 259:350–58
Eason ELE, Giampapa MS, Radick RR, Worden SP, Hege EK. 1992. *Astron. J.* 104:1161–73
Egedal J, Fox W, Katz N, Porkolab M, Øieroset M, et al. 2008. *J. Geophys. Res.* 113:A12207
Emslie AG, Dennis BR, Holman GD, Hudson HS. 2005. *J. Geophys. Res.* (*Space Phys.*) 110:A11103
Emslie AG, Kucharek H, Dennis BR, Gopalswamy N, Holman GD, et al. 2004. *J. Geophys. Res.* (*Space Phys.*) 109:A10104
Emslie AG, Miller JA, Brown JC. 2004. *Ap. J.* 602:L69–72
Fárník F, Hudson H, Watanabe T. 1996. *Solar Phys.* 165:169–79
Favata F, Flaccomio E, Reale F, Micela G, Sciortino S, et al. 2005. *Ap. J. Suppl.* 160:469–502
Favata F, Micela G. 2003. *Space Sci. Rev.* 108:577–708
Favata F, Schmitt JHMM. 1999. *Astron. Astrophys.* 350:900–16
Feigelson ED, Garmire GP, Pravdo SH. 2002. *Ap. J.* 572:335–49
Fisher GH. 1989. *Ap. J.* 346:1019–29
Fisher GH, Canfield RC, McClymont AN. 1985. *Ap. J.* 289:434–41
Fisk LA. 1996. *J. Geophys. Res.* 101:15547–54
Fletcher L, Hannah IG, Hudson HS, Metcalf TR. 2007. *Ap. J.* 656:1187–96
Fletcher L, Hudson HS. 2008. *Ap. J.* 675:1645–55
Fletcher L, Warren HP. 2003. In *Energy Conversion and Particle Acceleration in the Solar Corona*, *Lect. Notes Phys.* 612, ed. L Klein, pp. 58–79. Berlin: Springer-Verlag
Frost KJ, Dennis BR. 1971. *Ap. J.* 165:655–59
Fuhrmeister B, Liefke C, Schmitt JHMM, Reiners A. 2008. *Astron. Astrophys.* 487:293–306
Fuhrmeister B, Schmitt JHMM. 2004. *Astron. Astrophys.* 420:1079–85
Fuhrmeister B, Schmitt JHMM, Wichmann R. 2004. *Astron. Astrophys.* 417:701–13
Gershberg RE, Shakhovskaia NI. 1983. *Ap. Space Sci.* 95:235–53
Getman KV, Feigelson ED, Micela G, Jardine MM, Gregory SG, Garmire GP. 2008. *Ap. J.* 688:437–55
Gold T, Hoyle F. 1960. *MNRAS* 120:89–105
Gopalswamy N, Thompson WT, Davila JM, Kaiser ML, Yashiro S, et al. 2009. *Solar Phys.* 259:227–54
Goswami JN, Marhas KK, Sahijpal S. 2001. *Ap. J.* 549:1151–59
Graffagnino VG, Wonnacott D, Schaeidt S. 1995. *MNRAS* 275:129–42
Grießmeier JM, Stadelmann A, Motschmann U, Belisheva NK, Lammer H, Biernat HK. 2005. *Astrobiology* 5:587–603
Grigis PC, Benz AO. 2004. *Astron. Astrophys.* 426:1093–101
Grigis PC, Benz AO. 2005. *Astron. Astrophys.* 434:1173–81
Grigis PC, Benz AO. 2006. *Astron. Astrophys.* 458:641–51
Grosso N, Montmerle T, Feigelson ED, André P, Casanova S, Gregorio-Hetem J. 1997. *Nature* 387:56–58
Güdel M. 2002. *Annu. Rev. Astron. Astrophys.* 40:217–61
Güdel M. 2004. *Astron. Astrophys. Rev.* 12:71–237

Güdel M, Audard M, Kashyap VL, Drake JJ, Guinan EF. 2003. *Ap. J.* 582:423–42
Güdel M, Audard M, Skinner SL, Horvath MI. 2002a. *Ap. J. Lett.* 580:L73–76
Güdel M, Audard M, Smith KW, Behar E, Beasley AJ, Mewe R. 2002b. *Ap. J.* 577:371–76
Güdel M, Benz AO. 1993. *Ap. J. Lett.* 405:L63–66
Güdel M, Benz AO, Schmitt JHMM, Skinner SL. 1996. *Ap. J.* 471:1002–14
Güdel M, Guinan EF, Skinner SL. 1997. *Ap. J.* 483:947–60
Güdel M, Linsky JL, Brown A, Nagase F. 1999. *Ap. J.* 511:405–21
Güdel M, Nazé Y. 2009. *Astron. Astrophys. Rev.* 17:309–408
Gunn AG, Doyle JG, Mathioudakis M, Houdebine ER, Avgoloupis S. 1994. *Astron. Astrophys.* 285:489–96
Haisch BM, Butler CJ, Foing B, Rodono M, Giampapa MS. 1990. *Astron. Astrophys.* 232:387–95
Haisch B, Strong KT, Rodono M. 1991. *Annu. Rev. Astron. Astrophys.* 29:275–324
Hallinan G, Antonova A, Doyle JG, Bourke S, Lane C, Golden A. 2008. *Ap. J.* 684:644–53
Handy BN, Acton LW, Kankelborg CC, Wolfson CJ, Bruner ME, et al. 1999. *Solar Phys.* 187:229–60
Hannah IG, Christe S, Krucker S, Hurford GJ, Hudson HS, Lin RP. 2008. *Ap. J.* 677:704–18
Hawley SL, Allred JC, Johns-Krull CM, Fisher GH, Abbett WP, et al. 2003. *Ap. J.* 597:535–54
Hawley SL, Fisher GH. 1992. *Ap. J. Suppl.* 78:565–98
Hawley SL, Fisher GH, Simon T, Cully SL, Deustua SE, et al. 1995. *Ap. J.* 453:464–79
Hawley SL, Pettersen BR. 1991. *Ap. J.* 378:725–41
Hayashi MR, Shibata K, Matsumoto R. 1996. *Ap. J. Lett.* 468:L37–41
Herbst E, Klemperer W. 1973. *Ap. J.* 185:505–34
Herbst E, van Dishoeck EF. 2009. *Annu. Rev. Astron. Astrophys.* 47:427–80
Heyvaerts J, Priest ER, Rust DM. 1977. *Ap. J.* 216:123–37
Houdebine ER, Foing BH, Doyle JG, Rodono M. 1993a. *Astron. Astrophys.* 274:245–64
Houdebine ER, Foing BH, Doyle JG, Rodono M. 1993b. *Astron. Astrophys.* 278:109–28
Houdebine ER, Foing BH, Rodono M. 1990. *Astron. Astrophys.* 238:249–55
Hudson HS. 1991. *Solar Phys.* 133:357–69
Hurford GJ, Krucker S, Lin RP, Schwartz RA, Share GH, Smith DM. 2006. *Ap. J. Lett.* 644:L93–96
Ilgner M, Nelson RP. 2006. *Astron. Astrophys.* 455:731–40
Imanishi K, Nakajima H, Tsujimoto M, Koyama K, Tsuboi Y. 2003. *Publ. Astron. Soc. Pac.* 55:653–81
Innes DE, Attie R, Hara H, Madjarska MS. 2008. *Solar Phys.* 252:283–92
Innes DE, Inhester B, Axford WI, Wilhelm K. 1997. *Nature* 386:811–13
Isobe H, Shibata K, Yokoyama T, Imanishi K. 2003. *Publ. Astron. Soc. Pac.* 55:967–80
Isola C, Favata F, Micela G, Hudson HS. 2007. *Astron. Astrophys.* 472:261–68
Jansen F, Lumb D, Altieri B, Clavel J, Ehle M, et al. 2001. *Astron. Astrophys.* 365:L1–6
Kahler S. 1977. *Ap. J.* 214:891–97
Kane SR, McTiernan JM, Hurley K. 2005. *Astron. Astrophys.* 433:1133–38
Kashyap VL, Drake JJ, Güdel M, Audard M. 2002. *Ap. J.* 580:1118–32
Khodachenko ML, Ribas I, Lammer H, Grießmeier JM, Leitner M, et al. 2007. *Astrobiology* 7:167–84
Kiplinger AL, Dennis BR, Frost KJ, Orwig LE, Emslie AG. 1983. *Ap. J. Lett.* 265:L99–104
Kliem B, Karlický M, Benz AO. 2000. *Astron. Astrophys.* 360:715–28
Kopp RA, Poletto G. 1984. *Solar Phys.* 93:351–61
Kosugi T, Dennis BR, Kai K. 1988. *Ap. J.* 324:1118–31
Kosugi T, Matsuzaki K, Sakao T, Shimizu T, Sone Y, et al. 2007. *Solar Phys.* 243:3–17
Krucker S, Battaglia M, Cargill PJ, Fletcher L, Hudson HS, et al. 2008. *Astron. Astrophys. Rev.* 16:155–208
Krucker S, Benz AO. 1998. *Ap. J. Lett.* 501:L213–16
Krucker S, Benz AO. 2000. *Solar Phys.* 191:341–58
Krucker S, Benz AO, Bastian TS, Acton LW. 1997. *Ap. J.* 488:499–505
Krucker S, Lin RP. 2008. *Ap. J.* 673:1181–87
Kulikov Y, Lammer H, Lichtenegger H, Penz T, Breuer D, et al. 2007. *Space Sci. Rev.* 129:207–43
Kundu MR, Jackson PD, White SM, Melozzi M. 1987. *Ap. J.* 312:822–29
Kundu MR, Pallavicini R, White SM, Jackson PD. 1988. *Astron. Astrophys.* 195:159–71
Kürster M, Schmitt JHMM. 1996. *Astron. Astrophys.* 311:211–29
Lacy CH, Moffett TJ, Evans DS. 1976. *Ap. J. Suppl.* 30:85–96

Laming JM, Drake JJ, Widing KG. 1996. *Ap. J.* 462:948–59
Lammer H, Lichtenegger HIM, Kulikov YN, Grießmeier JM, Terada N, et al. 2007. *Astrobiology* 7:185–207
Lang KR, Bookbinder J, Golub L, Davis MM. 1983. *Ap. J. Lett.* 272:L15–18
Lee T, Shu FH, Shang H, Glassgold AE, Rehm KE. 1998. *Ap. J.* 506:898–912
Lefèvre E, Klein KL, Lestrade JF. 1994. *Space Sci. Rev.* 68:293–96
Lestrade JF, Mutel RL, Preston RA, Phillips RB. 1988. *Ap. J.* 328:232–42
Lim J, White SM, Nelson GJ, Benz AO. 1994. *Ap. J.* 430:332–41
Lin RP, Dennis BR, Hurford GJ, Smith DM, Zehnder A, et al. 2002. *Solar Phys.* 210:3–32
Lin RP, Feffer TP, Schwartz RA. 2001. *Ap. J. Lett.* 557:L25–28
Linsky JL, Drake SA, Bastian TS. 1992. *Ap. J.* 393:341–56
Linsky JL, Wood BE. 1994. *Ap. J.* 430:342–50
Lu ET, Hamilton RJ. 1991. *Ap. J. Lett.* 380:L89–92
Lundin R, Lammer H, Ribas I. 2007. *Space Sci. Rev.* 129:245–78
Maggio A, Pallavicini R, Reale F, Tagliaferri G. 2000. *Astron. Astrophys.* 356:627–42
Marino A, Micela G, Peres G. 2000. *Astron. Astrophys.* 353:177–85
Mariska JT, Emslie AG, Li P. 1989. *Ap. J.* 341:1067–74
Massi M, Forbrich J, Menten KM, Torricelli-Ciamponi G, Neidhöfer J, et al. 2006. *Astron. Astrophys.* 453:959–64
Massi M, Menten K, Neidhöfer J. 2002. *Astron. Astrophys.* 382:152–56
Massi M, Ros E, Menten KM, Kaufman Bernadó M, Torricelli-Ciamponi G, et al. 2008. *Astron. Astrophys.* 480:489–94
Masuda S, Kosugi T, Hara H, Tsuneta S, Ogawara Y. 1994. *Nature* 371:495–97
Mathioudakis M, Doyle JG. 1990. *Astron. Astrophys.* 240:357–59
McKenzie DE, Hudson HS. 1999. *Ap. J. Lett.* 519:L93–96
McTiernan JM. 2009. *Ap. J.* 697:94–99
Mewaldt RA, Cohen CMS, Giacalone J, Mason GM, Desai MI, et al. 2008. In *Particle Acceleration and Transport in the Heliosphere and Beyond: 7th Annu. Int. Astrophys. Conf., AIP Conf. Proc.* 1039, ed. G Li, Q Hu, O Verkhoglyadova, G Zank, RP Lin, J Luhmann, pp. 111–17. New York: Springer
Miller JA, Cargill PJ, Emslie AG, Holman GD, Dennis BR, et al. 1997. *J. Geophys. Res.* 102:14631–60
Miller JA, Larosa TN, Moore RL. 1996. *Ap. J.* 461:445–64
Milligan RO, Gallagher PT, Mathioudakis M, Keenan FP. 2006. *Ap. J. Lett.* 642:L169–71
Mitra-Kraev U, Harra LK, Güdel M, Audard M, Branduardi-Raymont G, et al. 2005. *Astron. Astrophys.* 431:679–86
Montes D, Saar SH, Collier Cameron A, Unruh YC. 1999. *MNRAS* 305:45–60
Montmerle T, Grosso N, Tsuboi Y, Koyama K. 2000. *Ap. J.* 532:1097–110
Montmerle T, Koch-Miramond L, Falgarone E, Grindlay JE. 1983. *Ap. J.* 269:182–201
Morris DH, Mutel RL, Su B. 1990. *Ap. J.* 362:299–307
Mutel RL, Lestrade JF, Preston RA, Phillips RB. 1985. *Ap. J.* 289:262–68
Mutel RL, Molnar LA, Waltman EB, Ghigo FD. 1998. *Ap. J.* 507:371–83
Ness JU, Güdel M, Schmitt JHMM, Audard M, Telleschi A. 2004. *Astron. Astrophys.* 427:667–83
Neupert WM. 1968. *Ap. J. Lett.* 153:L59–64
Nordon R, Behar E. 2008. *Astron. Astrophys.* 482:639–51
Øieroset M, Phan TD, Fujimoto M, Lin RP, Lepping RP. 2001. *Nature* 412:414–17
Orrall FQ, Zirker JB. 1976. *Ap. J.* 208:618–32
Osten RA, Bastian TS. 2006. *Ap. J.* 637:1016–24
Osten RA, Bastian TS. 2008. *Ap. J.* 674:1078–85
Osten RA, Brown A, Ayres TR, Drake SA, Franciosini E, et al. 2004. *Ap. J. Suppl.* 153:317–62
Osten RA, Brown A, Ayres TR, Linsky JL, Drake SA, et al. 2000. *Ap. J.* 544:953–76
Osten RA, Drake S, Tueller J, Cummings J, Perri M, et al. 2007. *Ap. J.* 654:1052–67
Osten RA, Hawley SL, Allred JC, Johns-Krull CM, Roark C. 2005. *Ap. J.* 621:398–416
Ottmann R, Schmitt JHMM. 1996. *Astron. Astrophys.* 307:813–23
Pallavicini R, Tagliaferri G, Stella L. 1990. *Astron. Astrophys.* 228:403–25
Parker EN. 1988. *Ap. J.* 330:474–79

Parnell CE, Jupp PE. 2000. *Ap. J.* 529:554–59
Pearce G, Harrison RA, Bromage BJI, Pickering AGM. 1992. *Astron. Astrophys.* 253:601–3
Peres G, Serio S, Vaiana GS, Rosner R. 1982. *Ap. J.* 252:791–99
Peterson WM, Mutel RL, Güdel M, Goss WM. 2010. *Nature.* 463:207–9
Petrosian V, Donaghy TQ, McTiernan JM. 2002. *Ap. J.* 569:459–73
Petrosian V, Liu S. 2004. *Ap. J.* 610:550–71
Petschek HE. 1964. *NASA Spec. Publ.* 50:425
Priest E, Forbes T. 2000. *Magnetic Reconnection*. Cambridge, UK: Cambridge Univ. Press. 612 pp.
Ramaty R, Mandzhavidze N, Kozlovsky B, Murphy RJ. 1995. *Ap. J. Lett.* 455:L193–96
Reale F, Betta R, Peres G, Serio S, McTiernan J. 1997. *Astron. Astrophys.* 325:782–90
Reale F, Peres G, Orlando S. 2001. *Ap. J.* 557:906–20
Reeves KK, Seaton DB, Forbes TG. 2008. *Ap. J.* 675:868–74
Ribas I, Guinan EF, Güdel M, Audard M. 2005. *Ap. J.* 622:680–94
Rosner R, Vaiana GS. 1978. *Ap. J.* 222:1104–8
Saar SH, Bookbinder JA. 1998. In *Cool Stars, Stellar Systems, and the Sun*, ed. RA Donahue, JA Bookbinder, ASP Conf. Ser. 154, pp. 1560–66
Saint-Hilaire P, Benz AO. 2002. *Solar Phys.* 210:287–306
Saint-Hilaire P, Benz AO. 2005. *Astron. Astrophys.* 435:743–52
Salter DM, Hogerheijde MR, Blake GA. 2008. *Astron. Astrophys.* 492:L21–24
Samtaney R, Loureiro NF, Uzdensky DA, Schekochihin AA, Cowley SC. 2009. *Phys. Rev. Lett.* 103:105004
Scalo J, Kaltenegger L, Segura AG, Fridlund M, Ribas I, et al. 2007. *Astrobiology* 7:85–166
Schaefer BE, King JR, Deliyannis CP. 2000. *Ap. J.* 529:1026–30
Schmelz JT. 1993. *Ap. J.* 408:373–81
Schmelz JT, Kashyap VL, Saar SH, Dennis BR, Grigis PC, et al. 2009. *Ap. J.* 704:863–69
Schmitt JHMM, Favata F. 1999. *Nature* 401:44–46
Schmitt JHMM, Ness J, Franco G. 2003. *Astron. Astrophys.* 412:849–55
Schmitt JHMM, Reale F, Liefke C, Wolter U, Fuhrmeister B, et al. 2008. *Astron. Astrophys.* 481:799–805
Shibata K, Yokoyama T. 1999. *Ap. J. Lett.* 526:L49–52
Shibata K, Yokoyama T. 2002. *Ap. J.* 577:422–32
Shiota D, Isobe H, Chen PF, Yamamoto TT, Sakajiri T, Shibata K. 2005. *Ap. J.* 634:663–78
Shkolnik E, Walker GAH, Bohlender DA. 2003. *Ap. J.* 597:1092–96
Shu FH, Najita J, Ostriker E, Wilkin F, Ruden S, Lizano S. 1994. *Ap. J.* 429:781–96
Shu FH, Shang H, Glassgold AE, Lee T. 1997. *Science* 277:1475–79
Simnett GM. 1986. *Solar Phys.* 106:165–83
Skinner SL, Güdel M, Koyama K, Yamauchi S. 1997. *Ap. J.* 486:886–902
Skumanich A. 1985. *Austr. J. Phys.* 38:971–74
Slee OB, Nelson GJ, Stewart RT, Wright AE, Jauncey DL, et al. 1987. *MNRAS* 227:467–79
Smith DS, Scalo J, Wheeler JC. 2004. *Icarus* 171:229–53
Smith K, Güdel M, Audard M. 2005. *Astron. Astrophys.* 436:241–51
Smith K, Pestalozzi M, Güdel M, Conway J, Benz AO. 2003. *Astron. Astrophys.* 406:957–67
Stäuber P, Doty SD, van Dishoeck EF, Benz AO. 2005. *Astron. Astrophys.* 440:949–66
Stelzer B, Flaccomio E, Briggs K, Micela G, Scelsi L, et al. 2007. *Astron. Astrophys.* 468:463–75
Telleschi A, Güdel M, Briggs K, Audard M, Ness JU, Skinner SL. 2005. *Ap. J.* 622:653–79
Testa P, Drake JJ, Peres G. 2004. *Ap. J.* 617:508–30
Tsuboi Y, Koyama K, Murakami H, Hayashi M, Skinner S, Ueno S. 1998. *Ap. J.* 503:894–901
Umana G, Trigilio C, Hjellming RM, Catalano S, Rodono M. 1993. *Astron. Astrophys.* 267:126–36
Uzdensky DA. 2004. *Ap. Space Sci.* 292:573–85
van den Oord GHJ. 1990. *Astron. Astrophys.* 234:496–518
van den Oord GHJ, Doyle JG, Rodono M, Gary DE, Henry GW, et al. 1996. *Astron. Astrophys.* 310:908–22
van den Oord GHJ, Mewe R. 1989. *Astron. Astrophys.* 213:245–60
van den Oord GHJ, Mewe R, Brinkman AC. 1988. *Astron. Astrophys.* 205:181–96
Veronig A, Vrsnak B, Temmer M, Hanslmeier A. 2002. *Solar Phys.* 208:297–315
Veronig AM, Brown JC. 2004. *Ap. J. Lett.* 603:L117–20

Wargelin BJ, Kashyap VL, Drake JJ, García-Alvarez D, Ratzlaff PW. 2008. *Ap. J.* 676:610–27
Weisskopf MC, Tananbaum HD, Van Speybroeck LP, O'Dell SL. 2000. *SPIE* 4012:2–16
White SM, Franciosini E. 1995. *Ap. J.* 444:342–49
White SM, Kundu MR, Jackson PD. 1989. *Astron. Astrophys.* 225:112–24
Whitehouse DR. 1985. *Astron. Astrophys.* 145:449–50
Winebarger AR, Emslie AG, Mariska JT, Warren HP. 2002. *Ap. J.* 565:1298–311
Wolk SJ, Harnden FR Jr, Flaccomio E, Micela G, Favata F, et al. 2005. *Ap. J. Suppl.* 160:423–49
Wood BE, Harper GM, Linsky JL, Dempsey RC. 1996. *Ap. J.* 458:761–82
Woodgate BE, Robinson RD, Carpenter KG, Maran SP, Shore SN. 1992. *Ap. J. Lett.* 397:L95–98
Woods TN, Kopp G, Chamberlin PC. 2006. *J. Geophys. Res.* (*Space Phys.*) 111:A10S14
Yelenina TG, Ustyugova GV, Koldoba AV. 2006. *Astron. Astrophys.* 458:679–86
Zharkova VV, Gordovskyy M. 2005. *Astron. Astrophys.* 432:1033–47
Zweibel E, Yamada M. 2009. *Annu. Rev. Astron. Astrophys.* 47:291–332

Annual Review of Astronomy and Astrophysics

Volume 48, 2010

Contents

Indexes

Errata

An online log of corrections to *Annual Review of Astronomy and Astrophysics* articles may be found at http://astro.annualreviews.org/errata.shtml